University of Rome "La Sapienza"

FACULTY OF CIVIL AND INDUSTRIAL ENGINEERING

DEPARTMENT OF CIVIL, CONSTRUCTIONAL AND ENVIRONMENTAL

ENGINEERING

Ph.D. course in Environmental and Hydraulic Engineering

The impact of submersed aquatic vegetation on the development of river mouth bars

Doctoral Dissertation of:
Sara Lera

Tutor:
Prof. Roberto Guercio

Supervisor of the Doctoral Program:
Prof. Francesco Gallerano

February 2020

The impact of submersed aquatic vegetation on the development of river mouth bars

Doctoral Dissertation of:

Sara Lera

Tutor:

Prof. Roberto Guercio

Supervisor of the Doctoral Program:

Prof. Francesco Gallerano

Contents

2

List of Figures

1. Introduction

The new paradigm that earth surface processes and landforms cannot be well understood without considering biological influences is becoming increasingly recognized within the geomorphological community (*Howard and Mitchell, 1985; Naiman et al., 1988; Butler, 1995; Osterkamp and Hupp, 1996; Phillips, 1999; Gurnell et al., 2001; Stallins, 2006*).

Several studies have shown how biological organisms can control physical processes within the fluvial environment (*Tabacchi et al., 2000; Gurnell et al., 2005*) while other studies have focused on how hydrogeomorphic processes and landforms can control biological communities (*Naiman and Décamps, 1997; Steiger et al., 2005*). However, there remains limited understanding of how the biogeomorphic processes lead to the reciprocal adjustments between landforms and biological communities which define the landscape dynamics.

The analysis of the reciprocal linkage between biological communities and geomorphic processes and landforms can be called 'biogeomorphology'. Biogeomorphology is an emergent subdiscipline at the interface between ecology and geomorphology (*Viles, 1988; Naylor et al., 2002*) which promotes the development of new interdisciplinary concepts, models and methodological tools better adapted to break the biotic–abiotic dichotomy.

The biological influence on geomorphological processes is the influence of biota to create, maintain or transform their own geomorphological surroundings. In some cases, morphological processes are dominant over biological processes and therefore the biota have to adjust to their environment. In other cases, biological processes are dominant. The most interesting are those cases where there is a mutual interaction that leads to feedback coupling of processes.

When looking for these cases, it is important to examine the temporal and spatial scales of the mutually interacting processes. Geomorphological processes occur on time scales ranging from microseconds, relevant to turbulence, up to hundreds of millions of years for geological processes. The spatial scale range is similarly wide, from micrometers for

capillary flows in sediments up to the continental and global scales. Kirkby (1990) presents an example for the wide variety in scales for river systems (Figure 1). He presents a measure for the response rate of systems, defined as a diffusive transport rate, i.e. the ratio of the squared spatial dimension (m²) over the temporal dimension (y). The response rates for morphological processes such as sediment transport, channel morphology and river slope evolution are of the same size (about 103 m²/y), irrespective of the scale order. Hydraulic and hydrologic processes also share a response rate, which is larger than for morphological processes (about 106 m²/y). Vegetation growth has a relatively small response rate (about 1 m²/y), meaning that changes in vegetation patterns are a less dynamic landscape element than changes in morphology.
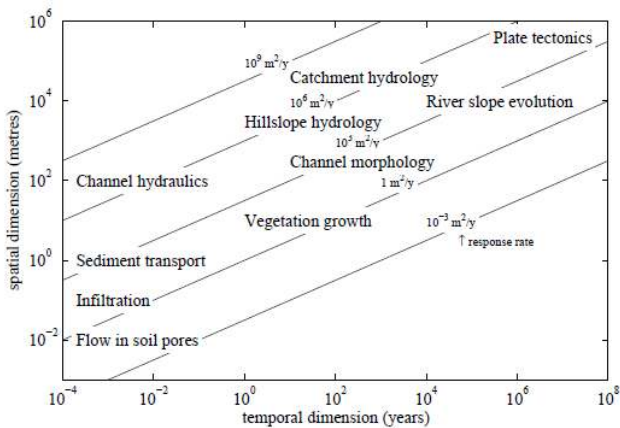
Figure 1. Temporal and spatial scales for geomorphological processes. The response rate indicates the evolution rate of the processes (Figure by Baptist, 2005).

As a general concept, this comparison of response rates may hold true for natural river systems. Consequently, this leads to the observation that for floodplain biogeomorphology,

morphodynamics is leading over vegetation dynamics and not the other way around. On the other hand, the reverse may be true in small, vegetation dominated streams.

Hydrologic, ecologic and geomorphic processes in a river basin are inherently coupled. On the one hand, natural vegetation patterns result from the interplay between climate, soils and topography; on the other, vegetation in turn exerts important controls on the hydrologic and geomorphic processes in the basin and contributes to the formation of landscape morphology over the long term. Vegetation is clearly an important factor in geomorphology.

Interactions between vegetation, hydrology and landscape development is inherently complex. It is conceivable that plant response to soil moisture deficit (*Porporato et al., 2001*), plant suitability to climate and soil conditions (*Laio et al., 2001; Porporato et al., 2003*), and coexistence of different species and functional types (*van Wijk and Rodriguez-Iturbe, 2002; Fernandez-Illescas and Rodriquez-Iturbe, 2004*) would have important implications for erosion rates and resulting landscape morphology. However, using a simple vegetation growth function seems to be a relevant preliminary strategy, although it will be applicable only in regions where plant growth is not limited by water. A number of fundamental questions in the interface between ecology and geomorphology remain to be explored.

1.1 Problem description

Coastal and estuarine modeling is concerned with understanding and predicting marine processes in coastal oceans and estuaries. One component of coastal and estuarine modeling is the prediction of sediment transport, including both fine sediments in shallow estuaries and coarser sediments in near-shore, wave-driven environments.

Over long time scales, sediment transport governs morphodynamics which strongly impacts coastal and estuarine flows. Unique to coastal and estuarine modeling is the connection to human influences particularly in densely populated coastal regions, where flows can be altered by coastal structures, dredging and sand nourishment operations, and

anthropogenic sources of contaminants and nutrients significantly impact coastal biogeochemistry.

Given that roughly 60% the world's population lives within 60 km of the coast and this is expected to rise to 75% within a few decades (*Rao et al., 2008*), accurate coastal and estuarine modeling is an essential component of efficient management for the sustainability of natural coastal systems and the development and improvement of sustainable urban infrastructure, particularly in the face of rapid urbanization of coastal cities and changing climate including sea-level rise.

This work focuses on the effect of vegetation on the development of a river mouth bar. The area in front of the mouth of deltaic distributary channels and rivers is a location where sediments accumulate and new landforms. At these locations sediment deposition can occur by growth of natural levees and channel elongation or by deposition and vertical aggradation of mouth bars.

Irrespective of their shape and evolution, these landforms are of paramount importance within the coastal landscape because, after emerging, they become deltaic islands and subaerial levees, which protect coastal communities (*Costanza et al., 2008*) and provide habitat for rich and productive ecosystems (*Gosselink and Pendleton, 1984*). In general, land naturally builds and erodes in relation to switching depocenters of rivers debouching in the ocean and sea level oscillations over long timescales, and storms and river floods over shorter timescales. In recent decades several river mouth landforms have been deteriorating because of sediment starvation triggered by the damming of large rivers, which reduces the flux of sediments to the ocean (*Syvitski et al., 2005*). In a period in which sea level rise is enhancing coastal erosion and flooding (*Nicholls and Mimura, 1998*), it is more important than ever to understand the physics of river mouth sediment deposits and how new land is built. In fact, deposition of sediments at river mouths not only can mitigate coastal erosion but it can also promote land expansion thus restoring anthropogenically modified coastlines (*Paola et al., 2011; Nittrouer et al., 2012; Edmonds, 2012, Kim et al., 2009; Kim, 2012*).

The formation of a bar, its size and shape depend on the intensity of sea and freshwater interaction processes taking place at the mouth of a river.

Bars are usually formed under similar environmental factors and the bar features can be traced at almost any river mouth. To form a bar in the mouth of a river, it is sufficient to

have a water flow that can transfer river sediments. The action of the river water flow and the sediment discharge builds up a background upon which the effect of other factors, such as waves, tidal currents, sea level rise, etc., deforming and shaping an already formed bar, is displayed. There is no doubt that passive factors as coastline configuration, sea-bottom relief underlying the bar, geological structure, etc., play no less an important role in the bars formation.

The growth of vegetation on the top of the sediment formations built up by a river flow enables them to consolidate. While hampering the further movement of sediments carried by the river flow, the vegetation cover facilitates the bar development, promotes the bifurcation of the river channel and contributes to the grows. This work is inspired by the sudden resurgence of the submersed aquatic vegetation (SAV) bed in the Chesapeake Bay (USA). Because the SAV bed occurs at the mouth of the Bay's main tributary (Susquehanna River), it plays a significant role in modulating sediment inputs from the Susquehanna to the Bay.

1.2 Objective and research questions

The objective of this thesis is to obtain a better understanding of the effect of vegetation on the development of river mouth bars. To reach this objective, four research questions are given below. Combined, these questions will set a next step in understanding vegetated flows and sediment transport in vegetated flows.

1. What are the factors influencing river mouth bars formation and development in absence of vegetation?

2. How can a numerical experiment be designed to make relevant observation on sediment transport in and around vegetation, combining long term processes (morphology) with small-scale effects (vegetation)?

3. What is the influence of submersed vegetation on the hydrodynamics and sediment transport of a river mouth bar?

4. Is it possible to explain bars growth patterns from submersed vegetation characteristics?

1.3 Outline

Chapter 2 gives the literature study and some background information starting with an overview of the effect of vegetation on the flow and specific aspects that influence the roughness and the turbulence. The literature gradually zooms into the fluid mechanics at the scale of an individual patch of vegetation examining turbulence and velocity profile of a flow through vegetation. This chapter also covers sediment transport mechanism, important for flow through vegetation. Furthermore, the state of the art of numerical models of flow-vegetation interaction is illustrated.

The method used for the numerical experiment is explained in chapter 3, focusing on the governing equations, some numerical aspects of the model and the vegetation model used in this study.

The numerical setup and the result analysis are explained in chapter 4. Figures and tables support the understanding of the numerical experiments.

The results are discussed in chapter 5 providing a comparison with previous river mouth models. In addition, seasonality effects on river mouth bar morphodynamics is analyzed. This chapter also reflects on the applicability of this results on the real case of Susquehanna Flats and other study systems. The last chapter gives the conclusions of this research.

2. Literature and theoretical frameworks

Vegetation is one of the important waterway components that play a key role in the flow and transport. Recently, developments in the field of river and coastal management have led to renewed interest in retaining the vegetation due to costly and ecological damaging procedures of removing channels vegetation.

Vegetation has shown positive impacts on water quality by removing pollution, increasing bed stability, assisting river restoration/rehabilitation, maintaining aquatic ecosystems, controlling flow velocity, improving rivers geomorphology, decreasing bed load and turbidity, diversifying habitat, as well as capturing and sequestering carbon (*Schulz et al., 2003; Sim et al., 2008; Jarvela, 2004; Afzalimehr and Dey, 2009; Arroyave and Crosato ,2010; Liu and Shen, 2008; Folkard, 2011*). Moreover, vegetation improves bank stability through sediment root binding, which increases the threshold shear stress, required to gradually wash the sediment.

Moreover, vegetation offers local flow resistance by reducing velocity, because it increases drag, while simultaneously decreasing the availability of shear stress for transport and erosion (*Thorne, 1990; Carollo et al,. 2002*). Ffolliott et al. (1995) have demonstrated that unprotected channels are more susceptible to erosion than channels protected by using a vegetative cover or lining. As soon as there is erosion in a channel, it becomes difficult to control it. The management of flood and river engineering requires the understand the effects of vegetation on the flow rate and sediment transport, which also determines the retardation in channels that are crucial in restoration design works (*Jarvela, 2005; Nepf and Ghisalberti, 2008*).

Chezy, Darcy-Waisbach and Manning formulations are equations generally used for flow resistance. A roughness coefficient which quantifies the flow resistance is considered in these formulas. Specifying the effect of vegetation in these relations has been attempted by researchers (*Jarvela, 2005; Afzalimehr and Dey, 2009*). However, the first analyses and discussion on vegetated channels was published in the last century by Chow (1959) and Barnes (1967), with definitions on semi-empirical methods for estimating the flow resistance.

The most widely used resistance measure is the flow resistance coefficient, Manning of vegetated channels. Gardiner and Dackombe (1983) have shown the use of traditional

methods for channel resistance as component parts, which uses experimental tables to value every element separately before determining the final value for the Manning's. However, the resistance tables used was very subjective and the estimated coefficient may be highly inaccurate (*Hey, 1979*) because flow resistance was presented as a function of the vegetation size, their location in the channel, the local flow conditions and structural properties (*Green, 2005).*

Darby (1999), Green (2005), and Jarvela (2005) however stated that when additional vegetation factors are introduced which include stems flexibility, plant height, and vegetation porosity, there is the likelihood that resistance tables become more inaccurate. Natural vegetation behaves different compared to artificial vegetation, for example, aquatic plants are difficult to bend during the day and period of growth because of the increase in the production of photosynthetic oxygen, which increases their boundary (*Powell, 1978*), seasonal vegetation effectiveness (*Fisher, 1992*) or age (*Pitlo, 1986*). Moreover, most figures and tables of resistant coefficients were not specifically designed for vegetated channels, and therefore, underestimate their resistance values (*Charnley, 1987*).

Afzalimehr and Dey (2009) have stated that the vegetation environment representing the area under the coverage of the vegetation, is a very important component in vegetated channels because it has significant impact on the turbulence of flow (*Folkard, 2005*), velocity (*Jarvela, 2004*), and sediment transport rate (*Zong and Nepf, 2010*). Nepf and Ghisalberti (2008) have stated that majority of the studies on vegetation focused on continuous beds, although in many natural settings, vegetation occurs in discontinuous patches of finite length. Afzalimehr and Dey (2009) has demonstrated different velocity profiles for some vegetation types, which conforms with previous studies (*Folkard, 2005; Wang et al., 2009*). However, several researches have demonstrated different turbulent behavior for various vegetation distribution and patches positions (*Zong and Nepf, 2010; Afzalimehr et al., 2010; Luhar et al., 2008*).
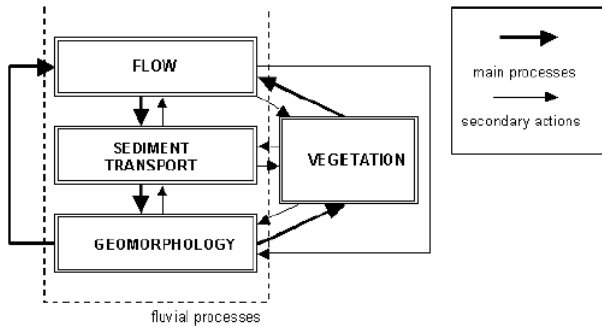
Figure 2. The influence of vegetation on fluvial processes (*Baptist, 2005*).

2.1 Flow through vegetation

2.2.1 Emergent vegetation

An emergent canopy fills the entire water depth H and typically penetrates the water surface.

This type of canopy occurs in tidal marshes, kelp forests, and seagrass meadows during periods of low tide.

Emergent canopies impose structure on both the mean and turbulent flow over the entire water column. The canopy dissipates eddies with scales greater than the stem scales, while contributing additional turbulent energy at these stem scales (Figure 3).

As a result, the dominant turbulent length scale within a canopy is shifted downward from analogous conditions without vegetation. In a channel with rigid vegetation, the integral length scale of the turbulence, is set by the smaller of the stem diameter or the average distance to the nearest neighboring stem, regardless of the water depth (*Tanino & Nepf, 2008*).
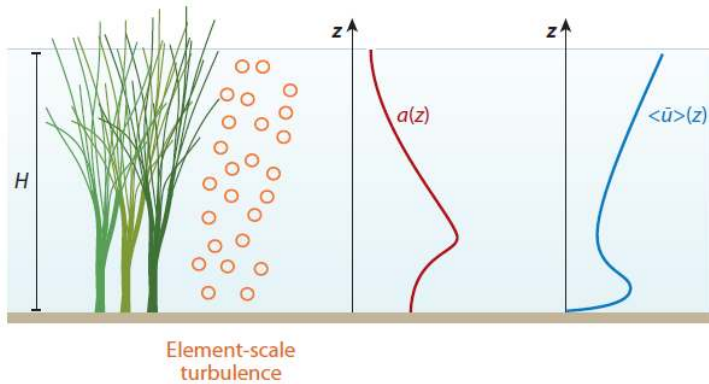
Figure 3. Emergent canopy of marsh grass, with vertical (*z*) profiles of leaf area index, *a*, and longitudinal velocity, ⟨*u⁻*⟩. The velocity profile varies inversely with *a*, creating a velocity maximum close to the bed, below the level at which branching begins.

In a square array of stems, the average spacing and the average nearest neighbor spacing are the same, but not in a random array. When the stem diameter is less than the average distance between stems, turbulence is generated within stem wakes (if the Reynolds number is sufficient) so that the length scale is equal to the stem diameter.

Otherwise, turbulence is generated within the pore channels. Even for solid volume fractions as low as 0.6%, the production of turbulence by the canopy exceeds the production by the bed shear over most of the flow depth (*Nepf et al., 1997; Burke & Stolzenbach, 1983; Lopez & Garcia, 1998*).

Therefore, the turbulence level cannot be predicted from the bed-friction velocity, as it can for

open-channel flow. Instead, it is a function of the canopy drag. Vortex generation by stem wakes and/or in pore channels drains energy from the mean flow (expressed in terms of canopy drag) and feeds it into the turbulent kinetic energy. If this conversion is 100% efficient, then the rate at which turbulent energy is produced, P_W, is equal to the rate at which mean flow energy is extracted, i.e., the rate of work done by the flow against canopy drag (*Raupach & Shaw, 1982*):

$$P_W = \frac{1}{2} C_D a(\bar{u})^3 \qquad\qquad\qquad \text{Eq. 1}$$

In fact, only the form drag is converted into turbulent kinetic energy. The viscous drag component is immediately dissipated to heat. For stiff canopies, i.e., most emergent canopies, and Re>200, the majority of the drag is form drag, and P_W is a reasonable approximation (*Tanino & Nepf, 2008*). In contrast, Nikora&Nikora (2007) suggested that for flexible canopies, which are typically submerged, the drag is predominantly viscous, and previous equation would be an overestimate of stem-scale turbulence production. The relative contributions of viscous drag and form drag depend on the morphology and alignment of the blades and stems within the canopy.

Within a homogenous emergent canopy, transport terms are negligible, and the wake production is balanced by viscous dissipation, ε, i.e., $P_W = \varepsilon$.

In addition, for turbulent kinetic energy, k, the dissipation rate within the canopy has the scale (*Tennekes & Lumley, 1972*)

$$\varepsilon \sim (\bar{k})^{3/2} l^{-1} \qquad\qquad\qquad \text{Eq. 2}$$

Connecting the equations, the turbulent intensity in the canopy is

$$\frac{\sqrt{(\bar{k})}}{(\bar{u})} \sim (C_D a l)^{1/3} \qquad\qquad\qquad \text{Eq. 3}$$

The turbulence length scale, l is set by the smaller of the stem diameter, d, and the nearest-neighbor stem spacing, S_n. In a canopy of low solid volume fraction, or specifically $S_n > d$, the turbulence intensity increases rapidly with increasing canopy density because $l = d$, and thus $al \approx d^2/S_n^2$. In a canopy of high solid volume fraction, $S_n < d$, the turbulence intensity increases more slowly because $l = S_n$, and thus $al \approx d/S_n$.

Within an emergent canopy, the momentum equation will generally simplify to a balance between potential forcing and canopy drag. Viscous stress is negligible compared to

vegetative drag over most of the depth, excluding a thin layer near the bed of a scale comparable to the stem diameter, d (*Nepf & Koch, 1999*). Then, the eddy length scale is small compared to the water depth, which limits the turbulence flux of momentum; i.e., the turbulence stresses are typically negligible. For example, from numerical experiments, the eddy scales are 1%–3% of the water depth, and turbulent stresses are only 2% of the total drag for aH = 0.1 (*Burke & Stolzenbach, 1983*). Similar ratios have been measured in model emergent canopies (*Nepf & Vivoni, 2000*). A notable exception occurs near the surface, as wind-generated stress can sometimes play a role in the momentum balance (J*enter & Duff, 1999*). Third, we assume that dispersive fluxes are negligible because the canopy density is commonly above the threshold ah > 0.1 suggested by Poggi et al. (2004). For steady, uniform flow, the momentum equation then reduces to

$$g \left(\frac{\partial H}{\partial x} + \sin \theta \right) = -\frac{1}{2} \frac{a C_D}{1 - \varphi} (\bar{u}) |(\bar{u})| = -\frac{(\bar{u})|(\bar{u})|}{L_c} \qquad \text{Eq. 4}$$

The hydrostatic pressure and potential gradients that drive the flow are not functions of the vertical coordinate, z. The right-hand side then must also be independent of z so that the velocity varies inversely with the frontal area, *a*, and in proportion to the canopy drag length scale, L_c.

For plants with a distinct basal stem, this produces a velocity maximum close to the bed because a is reduced below the level at which branching begins. A near-bed velocity maximum is often observed in the marsh grass *Spartina alterniflora* (*Leonard & Luther, 1999;, Leonard & Croft, 2006*). In contrast, the more vine-like *Atriplex portulacoides* has leaves that are more evenly distributed over depth, and the resulting velocity profile is uniform over depth (*Leonard & Reed, 2002*).

The velocity profile within an emergent canopy has a similar form.

When the velocity is normalized by its value at an arbitrary reference depth, denoted by the subscript ref, the normalized profiles collapse together, regardless of the absolute magnitude of the current. The shape of the normalized profile depends on the vertical distribution of L_c:

$$\frac{(\bar{u})}{(\bar{u})_{ref}} = \sqrt{\frac{L_c}{L_{c-ref}}} \sim \sqrt{\frac{(C_D a)_{ref}}{(C_D a)}} \qquad \text{Eq. 5}$$

where the right-most approximation holds in most salt- and freshwater wetlands canopies, for which the canopy solid volume fraction is small (ϕ < 0.1) so that $(1 - \phi) \approx 1$.

A similar velocity structure was confirmed by measurements in a coastal marsh (*Lightbody & Nepf, 2006*) and in the freshwater wetlands of the Everglades (*Huang et al., 2008*). The normalization provides an important tool for extrapolating a full velocity profile from records at a single vertical position.

An interesting nonlinear behavior emerges comparing flow conditions under different canopy densities but with the same potential and/or pressure gradient.

To include the no-canopy limit (i.e., bare bed), one must incorporate the bed resistance into the momentum balance.

Because the vegetation offers additional resistance, the velocity within the canopy is always less than that over a bare bed, and the velocity ratio, $(\bar{u})/u_b$, decreases as the vegetation density increases. Changes in turbulent kinetic energy with increasing vegetation density reflect the competing effects of the reduced velocity and the additional turbulence production in stem wakes. These opposing tendencies produce a nonlinear response in which the turbulence levels initially increase with increasing canopy density but decrease as a increases further. This nonlinear response was predicted numerically for flow through emergent vegetation (*Burke & Stolzenbach, 1983*) and within submerged roughness elements (*Eckman, 1990).* It has been observed in flume studies of flow through real stems of *Zostera marina* (*Gambi et al., 1990*). The enhanced turbulence levels in sparse canopies have important implications for canopy ecology.

It is commonly expected that dense patches of vegetation, because they damp flow and turbulence, are associated with muddification, an increase in fine particles and organic content of the underlying sediment relative to adjacent bare-bed conditions. Recently, van Katwijk et al. (2010) observed that sparse patches of vegetation are associated with sandification, a decrease in fine particles and organic matter, and they attribute this to higher levels of turbulence within the sparse patch, relative to adjacent bare regions. A transition from a tendency for sandification (elevated turbulence) to a tendency for muddification (diminished turbulence intensity) with increasing canopy density is consistent with the nonlinear model.

2.2.2 Submerged vegetation

The velocity within a submerged canopy has a range of behavior depending on the relative depth of submergence, defined as the ratio of flow depth H, to canopy height, h. The flow within the canopy is driven by the turbulent stress at the top of the canopy as well as by the gradients of pressure and gravitational potential (bed slope).

The relative importance of these driving forces varies with the depth of submergence (*Nepf & Vivoni, 2000*):

$$\frac{turbulent\ stress}{pressure\ gradient} \sim \frac{H}{h} - 1$$

Three classes of canopy flow can be defined: deeply submerged or unconfined (H/h > 10), shallow submergence (H/h < 5), and emergent (H/h = 1).
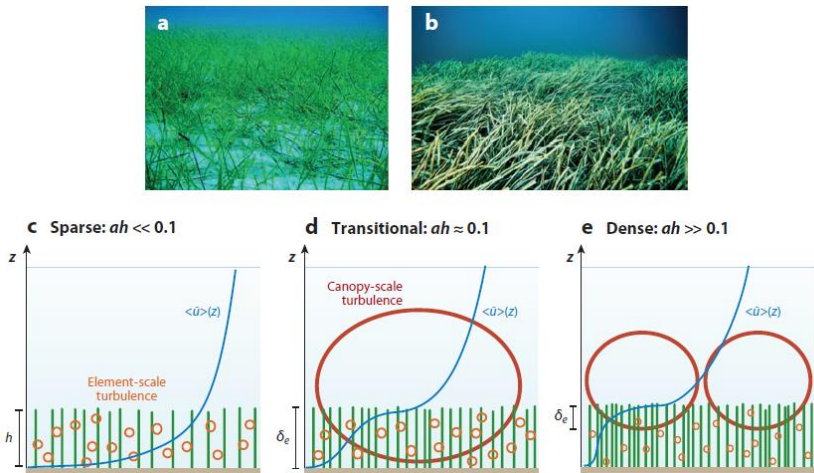
Figure 4. (a) The seagrass Cymodocea nodosa at low stem density. (b) The seagrass *Posidonia oceanica* at high stem density. Photos by Eduardo Infantes Oanes. Vertical (z)

profiles of longitudinal velocity and dominant turbulence scales are shown for (c) a sparse canopy (ah<<0.1), (d) a transitional canopy (ah ≈ 0.1), and (e) a dense canopy (ah>>0.1), where h is the submerged canopy height. For ah ≥ 0.1, a region of strong shear at the top of the canopy generates canopy-scale turbulence. Element-scale (stem-scale) turbulence is generated within the canopy.

 A great deal is known about unconfined canopy flow based on work in terrestrial canopies (*Raupach et al., 1996; Finnigan, 2000; Belcher et al., 2012*). When unconfined, the flow within a canopy is driven by the turbulent stress at the top of the canopy, i.e., by the vertical turbulent transport of momentum from the overflow, with negligible contribution from pressure gradients. The terrestrial canopy model can be applied to aquatic canopies that are deeply submerged. However, because of the limitation of light penetration, most submerged aquatic canopies occur in the range of shallow submergence $H/h<5$ (*Chambers&Kalff, 1985; Duarte, 1991*), for which both turbulent stress and potential gradients are important in driving flow in the canopy. For emergent conditions ($H/h=1$), flow is driven by the potential gradients, as described in the previous section. For a submerged canopy, there are two limits of behavior, depending on the relative importance of the bed drag and the canopy drag. If the canopy drag is small compared with the bed drag, then the velocity follows a turbulent boundary-layer profile, with the vegetation contributing to the bed roughness (sparse canopy; Figure 4c). If the canopy drag is large compared to the bed drag, the discontinuity in drag that occurs at the top of the canopy ($z = h$) generates a region of shear resembling a free shear layer with an inflection point near the top of the canopy (dense canopy; Figure 4d,e). From scaling arguments, Belcher et al. (2003) predicted that the transition between the sparse and dense regimes occurs at the roughness density $\lambda_f = ah = 0.1$. Numerical simulations by Coceal & Belcher (2004) suggest that the transition occurs at $L_c/h = 5$, which corresponds to $\lambda_f = 0.15$, for their parameter set ($C_D = 2$, $\phi = 0.25$). On the basis of measured velocity profiles in aquatic systems (*Nepf et al., 2007*), the profile exhibits a boundary-layer form with no inflection point if $C_Dah<0.04$. A pronounced inflection point appears at the top of the canopy for $C_Dah>0.1$. Because $C_D \approx 1$ in most of the studies considered, these limits are consistent with the scaling and numerical estimates given above.

For dense canopies, Raupach et al. (1996) demonstrated a similarity between canopy shear layers and free shear layers. In a free shear layer, the velocity profile contains an inflection

point, which triggers a flow instability that in turn leads to the generation of Kelvin-Helmholtz vortices (*Brown & Roshko, 1974; Winant & Browand, 1974*). These structures dominate the transfer of momentum between the high-speed and low-speed streams, and their size sets the length scale of the shear layer. For dense submerged canopies (ah≥0.1), the momentum absorption by the canopy is sufficient to produce an inflection point in the velocity profile, which, as in free shear layers, leads to the generation of Kelvin-Helmholtz vortices (Figure 4d,e). These vortices are called canopy-scale turbulence to distinguish it from the much-larger boundary-layer turbulence, which may form above a deeply submerged or unconfined canopy, and the much smaller stem-scale turbulence.

Over a deeply submerged canopy (H/h>10), the canopy-scale vortices are highly three-dimensional owing to their interaction with the larger boundary-layer turbulence, which stretches the canopy-scale vortices, enhancing secondary instabilities (*Fitzmaurice et al., 2004, Finnigan et al., 2009*). However, with shallow submergence (H/h≤5), which is common

in aquatic systems, larger-scale boundary-layer turbulence is not present, and the canopy-scale vortices dominate the turbulence field, both within and above the canopy (*Ghisalberti & Nepf, 2005; 2009*). For shallow submergence, the canopy-scale turbulence is also more coherent than that observed with deeply submerged conditions. However, in both cases, the canopy-scale vortices dominate the vertical transport at the canopy interface (*Gao et al., 1989; Finnigan, 2000; Ghisalberti & Nepf, 2002*).

In a free shear layer, the vortices grow continually downstream, predominantly through vortex pairing (*Winant&Browand, 1974*). In canopy shear layers, however, the vortices reach a fixed scale and a fixed penetration into the canopy (δ_e in Figure 4d,e) at a short distance from the canopy's leading edge (*Ghisalberti & Nepf, 2004*). On the basis of measurements with a flexible model of the seagrass *Z. marina* (a = 5.7 m−1), a fixed shear-layer scale is reached at a distance of 10h from the leading edge of the meadow (*Ghisalberti, 2000*). The fixed vortex and shear-layer scale is reached when the shear production that feeds energy into the canopy-scale vortices is balanced by dissipation by canopy drag. This energy balance predicts the following length scale, which has been verified by laboratory observations (*Nepf et al., 2007*):

$$\delta_e = \frac{0.23 \pm 0.6}{c_D a}$$ Eq. 6

In the range C_Dah = 0.1 to 0.23, the shear-layer vortices penetrate to the bed, δ_e=h, creating a highly turbulent condition over the entire canopy height (Figure 4d). At higher values of C_Dah, the canopy-scale vortices do not penetrate to the bed, δ_e <h (Figure 4e).

The scaling $\delta_e \sim a^{-1}$ has been observed in flows near porous layers over a wide range of physical scales, from granular beds to terrestrial forests and urban canopies (*Ghisalberti, 2009*). However, the scale relation must break down when $(C_Da)^{-1}$ approaches the scale of the canopy elements, *d*, because a is defined only as an average over multiple elements. For rigid cylinders, when $(C_Da)^{-1}$ is less than 2*d*, the penetration scale transitions to a constant $\delta_e \approx 2d$ (*White & Nepf, 2007*). The depth of submergence, H/h, can also affect the penetration length scale. For H/h < 2, δ_e is diminished, as interaction with the water surface diminishes the strength and scale of the vortices (*Nepf & Vivoni, 2000; Okamoto & Nezu, 2009*).

The penetration length, δ_e, segregates the canopy into an upper layer of strong turbulence and rapid renewal and a lower layer of weak turbulence and slow renewal (*Nepf & Vivoni, 2000*). Flushing of the upper canopy is enhanced by the canopy-scale vortices that penetrate this region (Figure 4e). In contrast, turbulence in the lower canopy (z < h − δ_e) is generated in stem wakes and has a significantly smaller scale, set by the stem diameters and spacing. Canopies for which δ_e/h<1 (Figure 4e) shield the bed from strong turbulence and turbulent stress.

Because turbulence near the bed plays a role in resuspension, these dense canopies are expected to reduce resuspension and trap sediment. Consistent with this, Moore (2004) observed that resuspension within a seagrass meadow was reduced, relative to bare-bed conditions, only when the above-ground biomass per unit area was greater than 100 gm^{-2} (dry mass). This biomass corresponds to ah = 0.4 (*Luhar et al., 2008*). The transition in near-bed turbulence and resuspension does not occur abruptly at C_Dah = 0.23 but occurs gradually with increasing C_Dah above this value, as the canopy-scale vortices are progressively pushed further from the bed (Nepf, 2011). Because of the reduced near bed turbulence, dense canopies can promote sediment retention. In sandy regions, which tend to be nutrient poor, the preferential retention of fines and organic material (muddification) enhances the supply of nutrients to the canopy so that dense canopies provide a positive feedback to canopy health in sandy regions. In contrast, in regions with muddy substrate,

sparse meadows ($C_Dah \leq 0.23$) may be more successful because the enhanced near-bed turbulence removes fines, leading to a sandier substrate.

2.2.3 Velocity profile

Sufficiently far above a submerged canopy (z > 2h), the velocity profile is logarithmic (*Kaimal & Finnigan, 1994*):

$$(\bar{u}) = \frac{u_*}{k} ln \left(\frac{z - z_m}{z_0} \right)$$ Eq. 7

with κ = 0.4 (von Karman constant). The horizontal average is not strictly needed above the canopy but is retained for consistency with the equations within the canopy. The friction velocity, u_*, is related to the Reynolds stress at the top of the canopy, $u_*^2 = < \overline{u'w'} > h$.

The parameters z_m and z_0 are the displacement and roughness heights, respectively, both of which depend on the canopy roughness density, *ah*. On the basis of studies with both model and real vegetation, a simple estimate for friction velocity is $u_* = [gS(H - h)]^{0.5}$, with $S = \partial H / \partial x + \sin \theta$ (*Murphy et al., 2007*). If the vegetation is flexible, then h is the mean deflected height of the canopy (*Jarvela, 2005*). However, if the depth of submergence is small, compared to the displacement height, the following estimator is more accurate: $u_* = [gS(H - z_m)]^{0.5}$ (*Nepf & Vivoni, 2000*).

Remembering that the penetration length scale, δ_e, describes the distance over which turbulent stress penetrates the canopy from above., similarly, the displacement height is the centroid of momentum penetration into the canopy (*Thom, 1971*). This similarity suggests the physically intuitive scaling

$$\frac{z_m}{h} \sim 1 - \frac{1}{2} \frac{\delta_e}{h} = 1 - \frac{0.1}{C_D ah}$$ Eq. 8

which has been confirmed for $ah \approx$ 0.2 to 3 (*Luhar et al., 2008*). For $ah > 1$, the displacement thickness tends toward $z_m \approx h$, indicating that essentially the entire canopy is cut off from the overflow. In addition, z_m goes to zero at $_{ah}$ = 0.1. When z_m = 0, the velocity profile has no inflection point (Figure 4c), consistent with the observation that $ah > 0.1$ is required to produce an inflection point in measured velocity profiles (Figure 4d, e).

The dependency of the roughness height, z_o, on the canopy density, ah, differs significantly above and below the threshold of ah = 0.1 (*Raupach et al., 1980; MacDonald et al., 1998; Jimenez, 2004; Luhar et al., 2008).

In the sparse-canopy range ($ah < 0.1$), the roughness height increases with increasing ah. In sparse canopies, the flow penetrates the full canopy so that z_o is proportional to the drag imparted by the full canopy, $C_D ah$, i.e., $z_o/h \sim C_D ah$.

In contrast, for dense canopies ($ah > 0.1$), the roughness height decreases with increasing ah. The effective height of the canopy, as seen by the overflow, is the penetration scale, δ_e. The roughness height depends on this effective height, rather than the canopy height, so that $z_o \sim \delta_e \sim a^{-1}$. For example, data summarized by Luhar et al. (2008) suggest that for $ah > 0.1$, $z_o = (0.04 \pm 0.02)a^{-1}$.

The logarithmic profile form is based on equilibrium turbulence such that dissipation and production are locally in balance (*Tennekes & Lumley, 1972*). Largely because of the vertical transport provided by the shear-layer structures, this condition is not met for some distance above the canopy, called the roughness sub-layer. For very shallow submergence, $H/h \leq 1.5$, the roughness sub-layer extends to the surface, and a logarithmic structure is not observed above the canopy.

The flow within a submerged canopy is driven by a combination of the turbulent, dispersive, and viscous stresses generated by the overflow, as well as the potential gradient associated with the hydrostatic pressure gradient and the bed slope. Below the penetration of turbulent and dispersive stress ($z < h - \delta_e$), conservation of linear momentum reduces to a balance between potential gradients and the sum of the canopy and the bed drag. Assuming that the canopy drag is much larger than the bed drag, this balance yields the following mean velocity:

$$(\bar{u}) = U_1 = \sqrt{\frac{2g(\frac{\partial H}{\partial x} + \sin\theta)}{C_D a}} \qquad \text{Eq. 9}$$

This is the same momentum balance observed for emergent canopies. So, if the canopy density a or drag coefficient C_D is a function of z, the velocity will vary inversely; i.e., the velocity will be highest where $C_D a$ is lowest.

In the upper canopy (h − δ_e < z < h), flow is driven by both potential gradients and turbulent stress. The stress-driven component is derived by simplifying the momentum equation to a balance of the canopy drag and turbulent stress and modeling the turbulent stress with a mixing length model, $\overline{(w'u')} = l_m^2 (\partial < \bar{u} > \partial z)^2$ (*Inoue, 1963*).

This yields the exponential velocity profile observed in terrestrial canopies. In aquatic canopies, the potential-driven component is also important in the upper canopy. Combining the stress driven and potential-driven components, the upper canopy velocity profile is

$$(\bar{u}) = U_1 + (U_h - U_1)\exp[-K_u(b-z)] \qquad \text{Eq. 10}$$

with U_h = $(\bar{u})$ at the top of the canopy, and constant K_u = β /l_m, with β = u_* /U_h. It is physically intuitive that the mixing length should be related to the penetration of shear-layer vortices into the canopy.

For rigid canopies in water, β = 0.24 $\pm$ 0.02 (*Ghisalberti & Nepf, 2005*), which predicts K_u = (8.7 $\pm$ 1.4)$C_D a$. This predicted value agrees with the observed decay scale constant, K_u = (9 $\pm$ 2)$C_D a$, extracted from measured velocity profiles in Ghisalberti (2005). In the dense canopy limit, β has no dependency on the canopy density (*Ghisalberti & Nepf, 2005*), but it declines as the transition to the sparse canopy limit (*ah*<0.1) is approached, i.e., as the canopy-scale vortices diminish and eventually disappear (*Poggi et al., 2004b*). Flexible canopies display a lower value, β = 0.17 $\pm$ 0.01 (*Ghisalberti & Nepf, 2005*), consistent with the less efficient momentum transfer noted in Figure 5. Belcher et al. (2003) proposed the alternative $K_u = (2l_m^2 L_c)^{-1/3}$, with the approximation $l_m \sim h$.
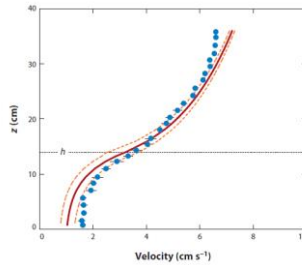
Figure 5. Measured velocity (*dots*) from Ghisalberti (2005). Predicted velocity (*solid line*) with confidence limits (*dashed lines*): H = 46.7 cm, h = 13.9 cm, S = 2.5 $\times$ 10^{-5}, a = 0.034 cm^{-1}, and C_D = 0.77 (measured). Above the meadow, the velocity is predicted from the logarithmic profile, with $u_* = [gS(H-h)]0.5$, $z_m = h - (1/2) \, \delta_e$, and $z_o = (0.04 \pm 0.02)a^{-1}$. Inside the meadow, the velocity is predicted with Uh taken from logarithmic fit.

To model the full velocity profile, both within and above the bed, researchers have combined the models for above-canopy and in-canopy profiles by matching the velocity at the top of the canopy (*Carollo et al., 2002; Abdelrhman, 2003*). Although this ignores the roughness sub-layer, for practical purposes the resulting profile is reasonably accurate. First, the velocity profile above the meadow (z>h) is estimated from the logarithmic profile. The logarithmic

profile provides the velocity at the top of the meadow, U_h, which is used to predict the velocity within the meadow (z < h). Other models for the complete velocity profile in regions with submerged aquatic vegetation have utilized different turbulence closure schemes (*Shimizu & Tsujimoto, 1994; Lopez & Garcia, 2001; Poggi et al., 2004; Defina & Bixio, 2005*), and some reflect the bending response of flexible vegetation (*Abdelrhman, 2007; Dijkstra & Uittenbogaard, 2010).*

2.2 Density and spatial distribution

Under natural conditions, plants often form spatially heterogeneous communities— patches which together with non-colonized spaces, or spaces colonized by different types

of vegetation, form irregular mosaics. Although the patchiness of aquatic vegetation is presently an important topic of ecological research (*Nikora, 2010a; Vandenbruwaene et al., 2011; Zong and Nepf, 2011*).

The occurrence of patches in channels may transform relatively two-dimensional open channel flow into complex three-dimensional flows (*Sukhodolov and Sukhodolova, 2010; Siniscalchi et al., 2012*). In fact, the flow patterns must be considered taking into account the large-scale turbulence associated with flow separation and wakes at the patch scale (pattern #7, Fig. 6), boundary layers and mixing layers developing at the patch side (pattern #8, Fig. 6b), as well as interacting vertical (pattern #9, Fig. 6a) and horizontal boundary layers at the patch mosaic scale (*Nikora, 2010; Zong and Nepf, 2010; Sukhodolov and Sukhodolova, 2012*).

Studies with submerged patches spanning the channel width showed that the upstream part of the patch diverts the flow upwards over the patch resulting in decelerating flow velocities in the canopy and flow acceleration above the patch.

This velocity difference contributes to the formation of a shear layer (*Ghisalberti and Nepf, 2004; Sukhodolova and Sukhodolov, 2012*) enhancing vertical turbulent transport of momentum (*Okamoto and Nezu, 2013; Zeng and Li, 2014*). Moreover, such a flow feature suggests that plants at patch edges experience significantly larger drag than plants in the middle of the patch as they are exposed to larger flow velocities (*Nikora, 2010; Siniscalchi et al., 2012*).
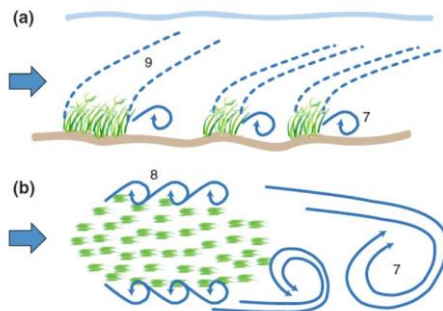
Figure 6. Flow patterns at patch scale: (a) side view considering patch mosaic structure and (b) plan view at patch scale (from *Nikora, 2010*)

The patch density and geometry are dominating factors for the turbulent flow field in and around the patches (*Green, 2005; Sukhodolov and Sukhodolova, 2012*). Increasing the vegetation density results in faster development of velocity and turbulence inside the patch due to the larger resistance compared to sparse densities (*Soulioutus and Prinos, 2011*). Moreover, these in-canopy flow features develop faster than the flow characteristics above the canopy (*Zeng and Li, 2014*).

Vegetated patches represent porous patches and this porosity affects the wake flow conditions. For example, the resulting wake from a porous patch is much longer compared to the wake generated by a similar solid obstruction as the bleed flow delays the onset of the von Karman vortex street (*Nepf, 2012*).

In the case of emergent patches, the flow is deflected sideways from the patch and a shear layer develops at the interface between the patch and the free flow (pattern #8 in Fig. 6b). The resulting horizontal mixing layer eddies dominate mass and momentum exchange and affect both the open channel and canopy turbulent flow features (*Nepf, 2012*). The horizontal penetration depth of these eddies depends, as for the submerged canopy case, on canopy density. However, due to the significant differences in flow geometry, both cases cannot be directly compared (*Nepf, 2012a*). The presence of more than one patch, patch mosaics, can result in a hydrodynamic interaction so that the upstream patch affects the flow features of the downstream patch. Flow interaction between vegetated patches such as flow acceleration depends on the ratio of patch size and distance between patches (*Vandenbruwane et al., 2001*).

2.3 Sediment transport in vegetated flows

Few studies have examined the influence of vegetation on flow and morphological changes. Bennett et al. (2008) extended their research (*Bennett et al., 2002*) by performing experimental and numerical simulations to investigate channel responses to finite patches, which consisted of emergent and circular cylinders. They showed that channel alterations

caused by both bank erosion opposite the patches and local scour pools near the patches were affected significantly by vegetation density. However, the authors did not measure bed elevation within the patch because of limitations in the experimental conditions.

Furthermore, Bouma et al. (2007) investigated spatial sedimentation patterns within patches in an intertidal flat. The patches comprised bamboo canes and two patch densities (low and high) were tested. Following 2 years of field monitoring, they observed that higher rates of erosion occurred in the high-density patch near its leading and lateral edges; sediment was deposited just beyond the scoured area observed near the leading edge. In contrast, there were no pronounced spatial patterns for erosion and deposition in the low-density patch, except for minor rates of erosion in the vicinity of the bamboo canes in the patch.

To investigate optimal stream restoration methods, Rominger et al. (2010) conducted a field experiment in a stream with sand substrate and meandering bends. Vegetation was added to point bars at the convex parts of the meandering channel. The authors observed that erosion occurred near the lateral edge of the vegetation, and it removed some of the added vegetation.

In addition, Follett and Nepf (2012) conducted laboratory experiments based on flow structures described by Zong and Nepf (2012) to investigate erosion patterns related to a circular patch of emergent vegetation placed mid-channel under flow conditions that were above the sediment motion threshold. The authors considered two patch densities and diameters that were much smaller than the channel width (i.e. the ratio of patch width to channel width was 0.08 to 0.18). Scour was observed within and around the patch and the degree of scouring increased with increasing patch density. This trend was significantly associated with turbulent kinetic energy within the patch.

2.4 An overview on technological development and numerical modeling

Models of physical processes in coastal environments have seen significant advances in the past two decades owing to increases in computational power and improved numerical methods including unstructured grids, model nesting, data assimilation, and model coupling.

In principle, a coastal model could directly compute the turbulent scales of motion and eliminate the need for a turbulence model if it were nonhydrostatic (since the turbulent scales are nonhydrostatic) and the grid resolution was sufficient to resolve the turbulent scales of

motion.

This could be accomplished with a direct-numerical simulation (DNS), for which the grid must resolve all of the turbulent scales of motion. However, DNS is not feasible in coastal flows given that the grid spacing must be on the order of the Kolmogorov dissipative scale which implies the need for an unrealistic number of grid points (*Pope, 2000*).

The computational cost can be alleviated with a large-eddy simulation (LES) in which the energy-containing eddies are resolved by the grid and the small, or subgrid-scale eddies, are parameterized with a so-called subgrid-scale (SGS) or subfilter-scale (SFS) model.

The degree to which the computational cost is reduced for LES when compared to DNS depends on the flow of interest. Near boundaries, the computational cost of LES is still extremely high because of the need to resolve the small near-wall turbulent scales that are proportional to the viscous wall unit.

To avoid the computational cost of resolving boundary layers, the LES can simulate the region away from the wall and parameterize the nearwall region and the associated stress with so-called wall-layer modeling (*Piomelli and Balaras, 2002*). Avoiding simulation of the near-wall region decreases the needed grid resolution roughly by a factor of 10 in each direction, leading to substantial savings in computational cost and the ability to simulate higher Reynolds numbers (*Piomelli and Balaras, 2002*).

The coastal models in use by the community today have been parallelized to some degree, either using distributed memory message passing techniques such as MPI and/or shared memory tools such as OpenMP.

It is well recognized that models that employ explicit methods in time or have simple matrix solves (e.g. symmetric and diagonally dominant) are typically easier to parallelize as they avoid the solution of potentially ill-conditioned systems of linear and nonlinear equations commonly found in implicit methods. However, implicit solvers have become much more sophisticated in recent years, with open-source packages, making them competitive for large-scale parallel computing.

Typical coastal models running large scale applications can scale to 100s or 1000s of cores on today's supercomputers.

As supercomputer architectures evolve, with Graphical Processing Unit (GPU) machines becoming more prevalent, and hybrid CPU/GPU machines coming online, the algorithmic techniques must also evolve.

Typical lower-order methods in use today in most codes will probably not scale well on these machines, due to low memory access to compute ratios. Higher-order methods may actually perform better, since more work is performed per cell, meaning more local memory access.

Another high-performance computing (HPC) arena that is rapidly evolving is the use of cloud computing. Cloud computing, at least as it pertains to physics-based simulations, is still in its infancy. Cloud computing opens up entirely new frontiers in making computing resources available and more affordable to a larger community and will most certainly have a larger role in the future of HPC.

2.5 Numerical models of flow-vegetation interactions

Several numerical models have previously been developed in order to represent flows through vegetation.

One of the most widely used approaches involves a canopy-scale momentum sink term, based upon the drag force exerted by the vegetation (*Fischer-Antze et al., 2001; Defina and Bixio, 2005*). This method requires prior knowledge of properties such as canopy density, projected plant area and a drag coefficient, and is therefore not suitable for investigating canopy-flow dynamics as it requires a priori assumptions regarding their nature. Such techniques are not suitable for investigating stem-scale turbulent energy dynamics.

To investigate the effect of turbulence production at the wake and leaf scales on turbulence structure and momentum transport, vegetation elements must be modelled at a scale where the vegetation diameter exceeds the spatial grid resolution of the model. This constraint on model resolution has meant that to date, most stem-scale models have

focused on high-resolution analysis of smaller-scale canopy properties and have not fully considered large or highly submerged canopies.

Stoesser et al. (2006) performed large eddy simulation (LES) experiments on an array of submerged cylinders using a spatially variable very fine grid resolution in order to fully capture the stem-scale turbulence. Their results agreed well with previous experimental results, as well as replicating the classical vortex regimes known to be present (horseshoe, von Karman, rib and roller vortices as well as trailing vortices from the vegetation tops). Subsequent work has developed this analysis and begun to use larger domains, enabling larger patch-scale analysis at stem-scale resolution.

Stoesser et al. (2010) undertook LES experiments on a patch of emergent vegetation using a combination of high-resolution Cartesian and curvilinear grids. They used a range of different vegetation densities and were able to investigate the structural changes to wake turbulence patterns caused by changes in vegetation density and found that these changes had a significant effect on turbulence statistics and flow resistance.

Whilst these stem-scale models can capture the fine turbulence structure with great accuracy, they do not include any treatment of flexible vegetation.

Submerged vegetation exhibits four different motion characteristics when exposed to a flow: (i) erect with no movement; (ii) gently swaying; (iii) strong, coherent swaying and (iv) prone (*Nepf and Vivoni, 2000*). Rigid models are therefore unable to capture the complex feedbacks between flow and vegetation, which influence canopy processes (*Nepf and Ghisalberti, 2008; Okamoto and Nezu, 2009).*

The first study to include flexible stems was conducted by Ikeda et al. (2001). They developed a biomechanical plant model for semi-rigid vegetation such as grasses and reeds (*Phragmites australis*) within a two-dimensional LES framework. However, as the model was only two-dimensional, it was not capable of capturing the full three-dimensional stem-scale energy dynamics.

Li and Xie (2011) extended this modeling approach to account for highly flexible vegetation, however, the spatial resolution of the model was sufficiently low that stems were not explicitly resolved and thus the model relied upon a priori assumptions regarding plant–flow interaction.

Abdelrhman (2007) developed a model for highly flexible stems, based on an N-pendula model to represent plant motion. However, this model had several limitations. Notably, it

used a simplified flow model which calculated the velocity at different heights based upon known

velocity profiles. Therefore, energy loss from the flow was represented by introducing a simple force balance into the flow equation, like that used to drive the plant model. The model was therefore able to replicate the familiar mean velocity profile but could not predict turbulent properties of the flow with accuracy.

This approach was further extended by Dijkstra and Uittenbogaard (2010) who included a parameterization of rigidity within the plant equations, allowing the model to be used more widely for plants exhibiting a range of flexibilities. The model was also used in conjunction within a one-dimensional Reynolds-averaged Navier–Stokes (RANS) flow model. The results showed that this vegetation model offered a significant improvement over rigid vegetation approximations, predicting plant positions and time-averaged flow characteristics. However, the model was very sensitive to the rigidity parameter, which is difficult to parameterize. Furthermore, the model was RANS-based and therefore unable to predict fully time-dependent turbulence characteristics.

Gac (2014) implemented a flexible vegetation model within a large eddy-based lattice Boltzmann model framework, which used a static version of the Euler–Bernoulli beam equation to calculate plant deflection (*Kubrak et al., 2008*). This method reproduced mean velocity profiles well, however, the treatment of plant motion did not account for inertial terms, solving only for a steady, static case at each time-step.

It is clear from the above discussion that, yet, a numerical model does not exist that can predict the time dependent interaction between flow and plant movement within a high-resolution, three-dimensional framework. Consequently, none of the above models are suitable for evaluating temporal vortex dynamics within vegetated flows.

3. Method

Delft 3D is used in this work to model numerically a river mouth bar evolution with and without submersed vegetation, using different vegetation heights and density. Delft 3D (*Roelvink and Van Banning, 1994; Lesser et al., 2004*) is an open-source computational fluid dynamics package that simulates fluid flow, waves, sediment transport, and morphological changes at different timescales.

An advantage of Delft3D is the full coupling of the hydrodynamic and morphodynamic modules so that the flow field adjusts in real time as the bed topography changes. The equations of fluid motion, sediment transport and deposition are discretized on a 3D curvilinear, finite-difference grid and solved by an alternating direction implicit scheme.

In this study, I used the three-dimensional formulation of the hydrodynamic and morphodynamic models implemented in Delft3D. Below the essential governing equations of the model are presented, and further details can be found in Lesser et al. (2004).

3.1 Governing equations

Delft 3D solves the Navier-Stokes equations for an incompressible fluid with the assumptions of shallow water and Boussinesq approximation. The mass-balance equation in Cartesian coordinates is:

$$\frac{\partial u}{\partial x} + \frac{\partial v}{\partial y} + \frac{\partial w}{\partial z} = 0 \qquad\qquad \text{Eq. 11}$$

where U, V and W are the averaged fluid velocity (m/s) along the x, y and z directions. The conservation of momentum equations for unsteady, incompressible, turbulent flow along the x-direction are given by:

$$\left(\frac{\partial U}{\partial t} + U\frac{\partial U}{\partial x} + V\frac{\partial U}{\partial y} + W\frac{\partial U}{\partial z}\right) - fV = -\frac{1}{\rho}\left[\frac{\partial p}{\partial x} + \left(\frac{\partial \tau_{xx}}{\partial x} + \frac{\partial \tau_{yx}}{\partial y} + \frac{\partial \tau_{zx}}{\partial z}\right)\right] + g_x \qquad \text{Eq. 12}$$

$$\left(\frac{\partial V}{\partial t} + U\frac{\partial V}{\partial x} + V\frac{\partial V}{\partial y} + W\frac{\partial V}{\partial z}\right) - fU = -\frac{1}{\rho}\left[\frac{\partial p}{\partial y} + \left(\frac{\partial \tau_{xy}}{\partial x} + \frac{\partial \tau_{yy}}{\partial y} + \frac{\partial \tau_{zy}}{\partial z}\right)\right] + g_y \qquad \text{Eq. 13}$$

$$\left(\frac{\partial W}{\partial t} + U\frac{\partial W}{\partial x} + V\frac{\partial W}{\partial y} + W\frac{\partial W}{\partial z}\right) = -\frac{1}{\rho}\left[\frac{\partial p}{\partial y} + \left(\frac{\partial \tau_{xz}}{\partial x} + \frac{\partial \tau_{yz}}{\partial y} + \frac{\partial \tau_{zz}}{\partial z}\right)\right] + g_z \qquad \text{Eq. 14}$$

where p, f, ρ, τ_{xx} and g are respectively the fluid pressure (N/m^2), Coriolis parameter (1/s), density (kg/m^3), fluid shear stress (N/m^2) and gravity acceleration (m/s^2). The vertical momentum equation is reduced to a hydrostatic pressure equation because of the shallow-water assumption. The standard k-ε closure model (*Rodi, 1984*) is used for the vertical eddy viscosity, and the horizontal eddy viscosity is computed with a large eddy simulation technique.

In its sediment transport and morphology modules, Delft3D calculates the amount of bed load and suspended load transport of non-cohesive and cohesive sediment, considering the interchange of sediment between the bed and water column. The suspended load transport is calculated by solving the three-dimensional diffusion-advection equation:

$$\frac{\partial c^i}{\partial t} + \frac{\partial U_x c^i}{\partial x} + \frac{\partial U_y c^i}{\partial y} + \frac{\partial (w - w_s^i)c^i}{\partial z} = \frac{\partial}{\partial x}\left(\varepsilon_{s,x}^i \frac{\partial c^i}{\partial x}\right) + \frac{\partial}{\partial y}\left(\varepsilon_{s,y}^i \frac{\partial c^i}{\partial y}\right) + \frac{\partial}{\partial z}\left(\varepsilon_{s,z}^i \frac{\partial c^i}{\partial z}\right) \quad \text{Eq. 15}$$

where c^i is the mass concentration of the i-th sediment fraction (kg/m^3), and w_s^i is the hindered sediment settling velocity of the i-th sediment fraction (m/s). $\varepsilon_{s,x}^i$, $\varepsilon_{s,y}^i$ and $\varepsilon_{s,z}^i$ are the sediment eddy diffusivities of the i-th sediment fraction (m^2/s) in the horizontal (x, y)

and vertical (z). The sediment eddy diffusivities are a function of the fluid eddy diffusivities calculated in the equations for fluid flow using horizontal large eddy simulation and grain settling velocity.

For cohesive sediment fractions, in case of erosion and deposition, the exchange between the water column and the bed are calculated with Partheniades-Krone formulations (*Partheniades, 1965*); for the non-cohesive fraction, sediment transport is computed following the method of Van Rijn (*Van Rijn, 1993*), in which the formulation depends on the diameter of the sediment in suspension.

3.2 Closure model

Turbulence closure is based on incorporation in the numerical model of the effect of sub-grid scale flow movements. The main effect of the sub-grid scale movements can be seen on a larger scale as mixing effects. These are incorporated in the model through internal turbulent stresses or Reynolds stresses. Modeling of the Reynolds stresses is known as the turbulence closure problem. In order to determine the Reynolds stresses τ_{ij} , the eddy viscosity concept as proposed by Boussinesq is used:

$$\tau_{ij} = -\rho v_t \left(\frac{\partial \bar{u}_i}{\partial x_j} + \frac{\partial \bar{u}_j}{\partial x_i} \right) - \frac{2}{3} \rho k \delta_{ij} \qquad \text{Eq. 16}$$

where x_i, x_j = x, y, z; k is the turbulent kinetic energy per unit mass ($k = \frac{1}{2} \bar{u}_i'^2$); δ_{ij} is the Kronecker delta and v_t is the turbulent or eddy viscosity. For determination of the Reynolds stresses it is now sufficient to specify the eddy viscosity. In contrast to the molecular viscosity v, the eddy viscosity v_t is not a fluid property but is dependent on the flow field. The second term on the right-hand side of equation (16) involving the Kronecker delta is usually neglected in large-scale numerical models.

The eddy viscosity is considered proportional to a turbulent velocity scale *U* and a turbulent length scale of the energy containing eddies *L*:

$$v_t \sim UL \hspace{4cm} \text{Eq. 17}$$

The horizontal eddy viscosity coefficient $(v_t)_h$ and diffusivity coefficient D_h are determined in Delft3D-FLOW by the user as direct input for the software module. In order to determine the vertical eddy viscosity and diffusivity coefficients $((v_t)_v$ and $D_v)$ four separate turbulence closure models are implemented in Delft3D-FLOW (*WL|Delft Hydraulics, 2001*):

1. Constant coefficient.

2. Algebraic turbulence closure model.

3. *k-L* turbulence closure model.

4. *k-ε* turbulence closure model.

In this work, the *k-ε* turbulence closure model is used.
In the *k-ε* model transport equations are solved for both the turbulent kinetic energy *k* and for the dissipation rate of turbulent energy *ε*. The transport equation for *k* and *ε* are given by (*Bijvelds, 2001*):

$$\frac{Dk}{Dt} = \frac{\partial}{\partial z}\left(\frac{v_t^v}{\sigma_t}\frac{\partial k}{\partial z}\right) + P_k + B_k - \varepsilon \hspace{3cm} \text{Eq. 18}$$

$$\frac{D\varepsilon}{Dt} = \frac{\partial}{\partial z}\left(\frac{v_t^v}{\sigma_t}\frac{\partial \varepsilon}{\partial z}\right) + P_\varepsilon + B_\varepsilon - c_{2\varepsilon}\frac{\varepsilon^2}{k} \hspace{2cm} \text{Eq. 19}$$

where σ_t is the Prandtl/Schmidt number (Eq. 18), P_k is a production term, B_k is a buoyancy term and ε is the energy dissipation. The production term is given by:

$$P_k = v_t^v \left(\left(\frac{\partial u}{\partial z} \right)^2 + \left(\frac{\partial v}{\partial z} \right)^2 \right)$$

Eq. 20

and the buoyancy term is given by:

$$B_k = v_t^v \frac{g}{\rho \sigma_t} \frac{\partial \rho}{\partial z}$$

Eq. 21

and in Eq. 19, P_ε is the production term, B_ε is the buoyancy term and the last term is the energy dissipation, with $c_{2\varepsilon}$ a model coefficient. The production term P_ε is derived from P_k through:

$$P\varepsilon = c_{1\varepsilon} \frac{\varepsilon}{k} P_k$$

Eq. 22

and the buoyancy term B_ε is derived from B_k through:

$$B_\varepsilon = c_{1\varepsilon} \frac{\varepsilon}{k} (1 - c_{3\varepsilon}) B_k$$

Eq. 23

where $c_{1\varepsilon}$ and $c_{3\varepsilon}$ are model coefficients.

The model coefficients in the k-ε model are prescribed by (*WL/Delft Hydraulics, 2001*):

$$c_{1\varepsilon} = 1.44$$

Eq. 24

$$c_{2\varepsilon} = 1.92$$

Eq. 25

$$c_{3\varepsilon} = \begin{cases} 1.0 & for\ R_i \geq 0, \\ 0.0 & for\ R_i < 0 \end{cases}$$

Eq. 26

From k and ε the mixing length L and eddy viscosity v_t^v are determined. The mixing length follows from:

$$L = c_D \frac{k^{3/2}}{\varepsilon}$$

Eq. 27

The mixing length in the k-ε model is a property of the flow field and no damping functions are needed in case of stratification.

For strongly stratified flows a suitably chosen constant ambient eddy viscosity is important because the eddy viscosity computed by the turbulence models from shear production reduces to zero in these cases. Layers are then decoupled (frictionless), disturbances are hardly damped and erosion of the stratification reduces to molecular diffusion (*WL/Delft Hydraulics, 2001*).

The vertical turbulent or eddy diffusivity D_v is directly derived from the eddy viscosity through:

$$D_v = \frac{v_t^v}{\sigma_t}$$

Eq. 28

in which σ_t is the Prandtl/Schmidt number. The numerical value for the Prandtl/Schmidt number depends on the substance for which the diffusion is applied. In general, the expression for the Prandtl/Schmidt number reads:

$$\sigma_t = \sigma_{t0} F_\sigma(R_i)$$

Eq. 29

in which σ_{t0} is a constant coefficient dependent on the substance and $F_\sigma(R_i)$ is a damping function.

3.3 Numerical aspects of the model

In Delft3D-FLOW orthogonal horizontal grids are used, with the grid points mapped in either rectangular, curvilinear or spherical coordinates in physical space. The grids are staggered grids, which means that water levels and velocities are computed in alternating grid points. The grid, with arrangement of the variables as used in Delft3D-FLOW, is called the Arakawa C-grid. The water level points are defined in the centre of a gridcell. The velocity components are defined on the grid cell faces and perpendicular to the cell face. Application of a staggered grid is favorable for reasons of accuracy and stability:

1. Boundary conditions can be implemented in a rather simple way.

2. In comparison with discretization on non-staggered grids, a smaller number of discrete state variables can be used to obtain the same accuracy.

3. The evaluation of the mass conservation principle is relatively simple with the combination of the water level point and the surrounding velocity points.

4. Staggered grids prevent spatial oscillations in the water levels.
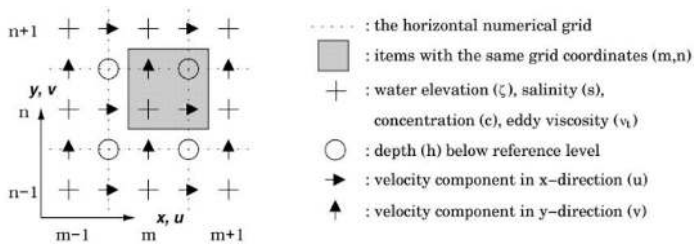
Figure 7. Horizontal numerical grid in Delft3D-FLOW; the staggered Arakawa C-grid.

The grid cells are mapped with grid coordinates (m, n). Figure 7 shows which variables have the same grid coordinates. Drying and flooding are represented by removing water elevation points when the water depth becomes smaller than a certain value (the threshold depth DRYFLC), while the surrounding velocity points are set to zero.

One of the common techniques used in large-scale applications of time-dependent, 3D models of flow in estuarine and coastal areas is the transformation from the (x, y, z) Cartesian coordinate system to the (x, y, σ) system, where σ is of the form z/H(x, y) and H(x, y) is the local depth.
Using the σ transformation the water column is divided into the same number of layers independently of the water depth. Figure 8 gives a definition of the σ coordinates compared to the normal Cartesian coordinates.
The σ transformation was first introduced in 1957 by Norman Phillips for use in meteorological forecasting. In meteorology σ coordinates are also called terrain following coordinates. In the 1970's it was introduced for use in hydrodynamic calculations, mainly for purposes of modeling flow circulation in seas and oceans. Since then it has been used for smaller scale applications. As these smaller scale applications exhibit relatively steep bed topographies the σ transformation yielded difficulties regarding the representation of density gradients (*Bijvelds, 2001*).
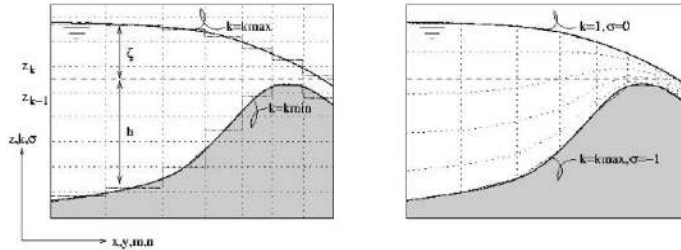
Figure 8. Cartesian (left) and σ (right) coordinates, definition of the vertical numerical grid. The indexing k of the layers in the z model runs in opposite direction from the σ model. Picture reproduced from Bijvelds (2001).

Leendertse (1990), in his discussion on ASCE (1988), says that σ transformation is commonly used, because it is easy to apply and greatly reduces the programming effort. Stelling & Van Kester (1994) state that the main advantage of the σ coordinates is the fact that they are fitted to both the moving free surface and the bottom topography. Furthermore, the terrain following coordinates allow an efficient grid refinement near the free surface (in the case of wind driven flow) and near the bed.

The choice between σ coordinates and alternatives that was made for the development of Delft3D-FLOW is discussed in WL|Delft Hydraulics, 1992.

With the σ coordinate system:

1. Computation routines become efficient and easy to implement because the number of layers in each vertical remains the same.

2. There is more freedom of choice for a vertical resolution near the bed and surface. Typical boundary layer processes (sediment transport, wind forcing) become easier to model.

3. Bed topography is represented boundary fitted.

4. Relative vertical resolution is independent of the water depth.

5. Mathematical consistency of the spatial discretization is reached when the layers are equally distributed in the vertical and the number of layers goes to infinity.

It can be added that memory requirements are relatively low with the σ coordinate system. Cartesian coordinates or z coordinates, as used by Bijvelds (2001), are defined in Figure 9. Although the vertical spacing Δz may vary in the vertical direction, each layer has the same thickness everywhere. Model variables are placed at the same level for the same layer (with exception of the bottom grid cells). A disadvantage is that this vertical discretization may lead to several inactive grid cells, which increases the computer memory requirements. The vertical layers are indexed by k. In σ coordinates k = 1 represents the first layer just below the free surface and k = k_{max} represents the layer just above the bed. The σ grid definition yields that k_{max} is a constant. In z coordinates k = k_{max} represents the first layer below the free surface and k = k_{min} represents the layer just above the bed. Both k_{max} as well as k_{min} are not constants in the z grid as the number of active layers in the z grid can change in time and space. Note that the indexing k in the z model runs in opposite direction from the σ model.
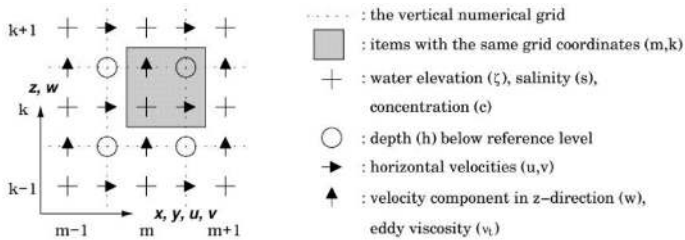
Figure 9. Vertical staggered numerical grid. Here the indexing k of the vertical points is according to the definition in the z grid. For the σ grid k runs in opposite direction.

Discretization in time can be performed with either explicit or implicit schemes. An explicit

scheme uses numerical values from previous time steps only in the current time step computations. In an implicit scheme values from previous time steps and from the current time step are used in the computations. Implicit schemes are rarely used for the horizontal flow computations, because they lead to a large system of algebraic equations.

In Delft3D-FLOW the momentum equations are solved simultaneously with the depth averaged continuity equation. An alternating-direction implicit (ADI) scheme is used for the discretization in time. This method allows large time steps without negative effects on the stability. The ADI method is a good compromise between explicit and implicit methods. It is based on the division of the time step in two equal parts.

At time t+1/2Δt the u velocity and water levels are computed (implicitly) along lines parallel to the x-axis and at time t +Δt the v velocities are computed along lines parallel to the y-axis. In order to reduce time step restrictions related to the propagation of free surface waves, the barotropic forcing is computed implicitly.

Horizontal convection/advection is computed explicitly. Implicit coupling of the velocity points in the horizontal direction is avoided and thus the efficiency of the numerical model is enhanced. For the z coordinate model, a first order upwind method is used for the spatial discretization that approximates the horizontal advection along a particle trajectory. Leendertse (1990), in his discussion on ASCE (1988), states that primitive upwind differencing of the advection terms introduce a very large amount of either eddy viscosity or diffusion in the computation.

In comparison to the standard first order upwind method, used in two-dimensional vertically integrated or three-dimensional applications, the interpolation of variables is performed with much less numerical diffusion in the present discretization (*Bijvelds, 2001*).

In the σ model for horizontal convection/advection a combination of second order central differencing and second order upwind differencing is used. This discretization is known to be of low artificial dissipation, in contrast to the first order upwind scheme. The two discretization of the advection terms are successively used in both stages of the ADI scheme.

The horizontal velocities of adjacent vertical layers are coupled by the vertical advection term and the vertical viscosity/diffusion term. The vertical advection is integrated implicitly in order to avoid time step restrictions related to stability, as the σ transformation can lead to very thin layers in shallow areas. This leads to tridiagonal

systems of equations in the vertical. In both the σ and the z model a second order central difference scheme is used for the discretization in vertical direction.

The horizontal diffusion or viscosity term in the momentum equation is computed explicitly in order to avoid coupling of the velocity points in the horizontal plane. In both the σ and the z model a second order central difference scheme is used for the spatial discretization. In the σ model the horizontal derivatives are computed along σ planes, whereas in the z model the derivatives are strictly horizontal. Vertical diffusion in the momentum equation is computed implicitly in both σ and z model; for the spatial discretization second order central differencing is employed.

While the momentum equation is mostly dominated by pressure gradients and bed friction, the transport equation is dominated by the advective and diffusive processes of the transported quantities. Accurate treatment of the advection and diffusion terms in the transport equation is therefore of major importance for simulating stratified flows (*Bijvelds, 2001*). To avoid negative concentrations of the scalar quantities a Forester filter, a local diffusion operator, is used. For horizontal advection in the z model the explicit Van Leer II method is used, yielding an extra time step restriction. This method is based on a first order upwind scheme, with which positive monotonic solutions are guaranteed, combined with a non-linear anti-diffusive addition. In the σ model the Cyclic method is used, based on an implicit time integration of both advection and diffusion. For the spatial discretization a summation of a third order upwind scheme and a second order central scheme is used.

The vertical advection is integrated implicitly in both the σ and the z model, in order to avoid time step restrictions related to stability. In both the σ and the z model a second order central scheme is used for the discretization in space.

The horizontal diffusion is computed explicitly in the z model in order to avoid coupling of the velocity points in the horizontal plane. In the z model the derivatives are computed along strictly horizontal planes. In the σ model the horizontal derivatives are computed along σ planes by default. However, in the σ model the diffusive fluxes can either be computed with the original spatial discretization, or the Stelling & Van Kester method can be used in which the horizontal fluxes are evaluated along horizontal planes.

Vertical diffusion is discretized by using an implicit second order central approximation for the diffusive fluxes in both the z and σ model.

3.4 Vegetation model

The impact of vegetation on the flow is generally expressed as an effect on the hydraulic bed roughness and flow resistance. Delft3D provides the opportunity to insert different classes of roughness inside the computational domain of the model to account for the effect of vegetation. One method to model vegetation is using Baptist's formulation (*Baptist et al., 2005*), where vegetation is represented as rigid cylinders characterized by stem diameter D, height H_v, density m and drag coefficient C_D. Baptist et al. (2007) derived an expression for the Chézy coefficient by applying genetic programming to the results of a 1DV k–ε turbulence model developed by Uittenbogaard (2003).

This model solves a simplification of the 3D Navier-Stokes equation for horizontal flow conditions. Starting from Uittenbogaard (2003), to include the effects of vegetation in the k–ε turbulence closure, some additional assumptions have been included by Baptist:

(a) the decrease of the available cross-section for the vertical exchange of momentum, turbulence kinetic energy, and turbulent dissipation,

(b) the drag force exerted by the plants in the horizontal direction,

(c) an additional turbulence production term due to vegetation, and

(d) an additional turbulence dissipation term due to vegetation (for more information see *Baptist et al., 2007*).

In the presence of vegetation, the velocity profile of the flow is assumed to be divided into two zones: inside the vegetated patch where flow velocity is constant, and above the vegetation where the velocity profile increases logarithmically from the constant value.

When vegetation is completely submerged, the total shear stress τ_t is given by the sum of the bed shear stress τ_b and the component due to the vegetation τ_v:

$$\tau_t = \rho ghi = \tau_b + \tau_v \qquad \text{Eq. 30}$$

$$\tau_b = \frac{\rho g}{C_b^2} u_v^2 \qquad \text{Eq. 31}$$

$$\tau_v = \frac{1}{2} \rho C_D m H_v u_v^2 \qquad \text{Eq. 32}$$

$$m = nD \qquad \text{Eq. 33}$$

where ρ is the water density, g is the gravitational acceleration, h is the water depth, i is the water surface slope, C_D is the bottom Chezy coefficient, C_b is the drag coefficient of the vegetation, m is the vegetation density, H_v is the vegetation height, n is the number of stems per unit area, D is the stem of the diameter ,and u_v is the uniform velocity component.

Taking in account these equations, the uniform velocity obtained is:

$$u_v = \sqrt{\frac{hi}{C_b^{-2} + (2g)^{-1} C_D m H_v}} \qquad \text{Eq. 34}$$

Defining the vegetated bed bottom shear stress as:

$$\tau_{bv} = f_s \tau_t$$
Eq. 35

where f_s is the reduction factor, and replacing Eq. 34 in Eq. 31:

$$f_s = \frac{1}{1 + \frac{C_D H_v C_b^2}{2g}}$$

Eq. 36

Combining Eq. 31 with Eq. 35, the equation obtained is given by:

$$\tau_{bv} = f_s \frac{\rho g}{C_{rs}^2} \bar{u}^2$$

Eq. 37

where C_{rs} is the total Chézy friction value for submerged vegetation:

$$C_{rs} = \sqrt{\frac{1}{C_b^{-2} + (2g)^{-1} C_D m H_v}} + \frac{\sqrt{g}}{k} \ln\left(\frac{h}{H_v}\right)$$

Eq. 38

in which k is the Von Karman constant (k = 0.4).

In the case of partially submerged vegetation, following the same procedure for fully submerged vegetation and adding bed shear stress τ_b and the shear stress due to the vegetation drag τ_v in Eq. 30:

$$ghi = \left(\frac{1}{2} C_D m h + \frac{g}{C_b^2}\right) u_v^2$$

Eq. 39

For partially submersed vegetation, $u_v = \bar{u}$, where $\bar{u}$ is the depth average flow velocity. Combining Eq. 31 and Eq. 34, the bed shear stress due to the flow velocity through the vegetation, $\tau_{bv,ns}$, becomes:

$$\tau_{bv,ns} = f_{ns}\tau_t \qquad \text{Eq. 40}$$

$$f_{ns} = \frac{1}{1 + \frac{C_D m h C_b^2}{2g}} \qquad \text{Eq. 41}$$

The main difference between the two cases of submerged and emergent vegetation is in the reduction factor which in the first case includes the vegetation height, H_v (Eq. 36), while in the second case contains the water depth, h (Eq. 41).

The representative Chézy value for non-submerged vegetation is defined by:

$$C_r = \frac{u_v}{\sqrt{hi}} \qquad \text{Eq. 42}$$

Introducing Eq. 34 in Eq. 42 the Chézy roughness coefficient for non-submerged vegetation becomes:

$$C_r = \sqrt{\frac{1}{C_b^{-2} + (2g)^{-1}C_D m H_v}} \qquad \text{Eq. 43}$$

Therefore in Eq. 38 the first term on the right-hand side equals the representative roughness for the partially submerged vegetation if $h = h_v$. Moreover, the value of C_{rs} is higher than the value of C_r leading to a smaller resistance for fully submerged vegetation. Further details can be found in Baptist et al. (2005).

Baptist's equation has been widely tested with field data and through laboratory experiments with natural and artificial vegetation (*Arboleda et al., 2010*). In addition, many experiments have compared the predicted results with experimental data, finding a good fit (*Crosato and Saleh, 2011; Arboleda et al., 2010*). Crosato and Saleh (2011) provide another validation of the Baptist's equation on the effects of floodplain vegetation on river planform.

To account for vegetation flexibility, in this work I followed the approach for large-scale morphodynamic models described by Dijkstra (2008). I chose a height and a drag coefficient of rigid vegetation equal to that of flexible plants under similar conditions, because the flow pattern is analogous and the sediment transport is governed by hydrodynamics, as shown in Dijkstra (2008) over a broad range of vegetation densities, flow speeds, and depths. A preliminary sensitivity test was conducted to assign deflected height and equivalent drag coefficient values, to obtain a very similar flow condition through rigid rods to the flow through flexible vegetation. Preliminary results further showed that the equivalent drag coefficient does not vary significantly over the flow range examined in our work, therefore we used only a single constant value.

4. The impact of submersed vegetation on the development of river mouth bars

4.1 Introduction

The process of river mouth bar evolution is one of the main mechanisms of delta formation, since mouth bars represent the smallest dynamic units in delta morphology. They occur when a sediment-laden river flow drains into a basin, where flow momentum and velocity decrease, promoting sediment deposition. The configuration of the resulting deposits reflects the interaction of multiple mechanisms and processes, including river-mouth geometry, grain size, and the effect of waves, tides, vegetation, and water-level variations (*Axelsson, 1967*).

Many studies focus on the entire topological structure of the delta (*Sun et al., 2002; Overeem et al., 2005; Fagherazzi and Overeem, 2007; Jerolmack and Swenson, 2007; Edmonds et al., 2009, 2011; Canestrelli et al., 2010; Edmonds and Slingerland, 2010; Geleynse et al., 2011; Edmonds, 2012*) and others analyze the process of river mouth bar formation and evolution in relation to parameters that contribute to morphological modeling (*Bates, 1953; Wright, 1977; Wang, 1984; Edmonds and Slingerland, 2007; Nardin and Fagherazzi, 2012; Esposito et al., 2013; Nardin et al., 2013*). For example, Wright and Coleman (1974) analyzed maps and field observations to highlight the variability of morphodynamic processes and suggested a focus on the relationship between morphology and dominant natural processes.

The conceptual model of river mouth bar evolution proposed by Edmonds and Slingerland (2007) identifies the stages of development: initial sediment deposition, progradation and aggradation of the bar until progradation ceases, then channel formation and bifurcation. This conceptual model is based on numerical results and validated by Esposito et al. (2013) with field data from the Mississippi River's bird's foot delta. Researchers have analyzed the morphology of river mouth deposits under the influence of waves (*Wright and Coleman, 1974; Jerolmack, 2009; Geleynse et al., 2010; Nardin et al., 2013*), since waves and the direction from which they derive play an important role in sediment distribution (*Nardin*

and Fagherazzi, 2012), along with tidal processes (*Lanzoni and Seminara, 2002; FitzGerald et al., 2006; D'Alpaos et al., 2007; De Swart and Zimmerman, 2009; Leonardi et al., 2013*). The presence of submersed aquatic vegetation (SAV) modifies hydrodynamics and sediment transport processes, and therefore also the morphological evolution of river mouth bars. Generally aquatic vegetation represents an additional hydraulic resistance to the flow; because flow diminishes in response, vegetation generally increases sediment deposition and reduces erosion (*Nepf, 1999*). There are exceptions to this general statement, especially at low vegetation densities. Resuspension was not repressed relative to an uncovered bed for sparse meadows in one study (*Moore, 2004*), while erosion was enhanced by sparse submerged patches in another study (*Lawson et al., 2012*). Furthermore, van Katwijk *et al*. (2010) observed that sparse submerged patches led to a sandification of meadow substrate because fines were dispersed by elevated turbulence. These trends are explained by the contribution of stem- and canopy-scale turbulence. As the stem density of a submerged meadow initially increases the turbulence within the meadow initially increases due to stem- and canopy-scale turbulence. Near-bed turbulence is only suppressed, supporting deposition, when the meadow density increases above a threshold value (*Luhar et al., 2008*). However, large, dense SAV beds capable of exerting a significant geomorphological influence generally promote net sediment deposition. The reduction of bed shear stress above this value limits suspended-sediment transport, supporting sediment deposition (*Lòpez and Garcia, 1998*).

Many studies focus on the effect of vegetation at river mouths with field data, such as in the Atchafalaya delta where Johnson et al. (1985) highlight vegetation enhanced sedimentation, and Rosen and Xu (2013) show that vegetation stabilizes deltaic land. Similarly, Larsen and Harvey, (2010) illustrates how vegetation and sediment transport interact in landscape evolution in the Everglades. Laboratory experiments have analyzed turbulent mixing and jet spreading in the presence of vegetation (*Mossa et al., 2017*) and how vegetated patches modify flow and sediment deposition *(Zong and Nepf, 2010)*, including turbulence (*Liu and Nepf, 2016*). Nardin and Edmonds (2014) explore the dynamics of deltaic river mouth sedimentation during a flood with numerical experiments and observe that the presence of vegetation on bars increases water flux through the channels, similar to observations in tidal-marsh channels (*Temmerman et al., 2007*).

The conceptual model of Edmonds and Slingerland (2007) provides a description of river mouth formation to analyze its evolution and to predict its ultimate location and shape

with the aim of better understanding delta distributary networks. Because aquatic vegetation plays a significant role in modulating sediment dynamics, this study aims to describe and quantify how vegetation modifies the hydrodynamic field and sediment transport in the morphological evolution of a river mouth bar.

To analyze the impact of submersed aquatic vegetation, I model numerically a river mouth bar formation and evolution, both without vegetation and with submersed vegetation with variable plant height and density. The interaction between vegetation and morphology is investigated with Delft3D (*Roelvink and van Banning, 1994; Lesser et al., 2004*), a coupled hydrodynamic and morphodynamic model.

This study is inspired by the submersed aquatic vegetation (SAV) bed on the Susquehanna Flats (Figure 10) in the upper Chesapeake Bay (USA). Susquehanna Flats is a broad shoal enclosed by deeper channels that forms a subaqueous delta located in front of the Susquehanna River mouth.

The Susquehanna basin comprises 43% of the Chesapeake Bay's drainage area (71.25 km^2) and is the main source of fresh water and sediment into the upper Bay. A rich assemblage of SAV occupies ~25 km^2 of the flats, including *Vallisneria americana*, *Myriophy spicatum*, *Hydrilla verticillata* and *Heteranthera dubia*.

Previous studies concerning Susquehanna Flats investigated SAV bed effects on environmental conditions with field measurements of SAV seasonal characteristics and current velocities in the presence and absence of vegetation (*Gurbisz et al., 2017*); Gurbisz and Kemp (2014) analyzed the resurgence of submerged plant bed after Tropical Storm Agnes (1972), and Gurbisz *et al.* (2016) studied the driving mechanisms of loss and resilience of the bed with field data and a hydrodynamic model that simulated flow and bottom stress on the Flats. Russ and Palinkas (2018) showed that sedimentation within the Flats is highest when the plants are present, on both seasonal and decadal timescales.
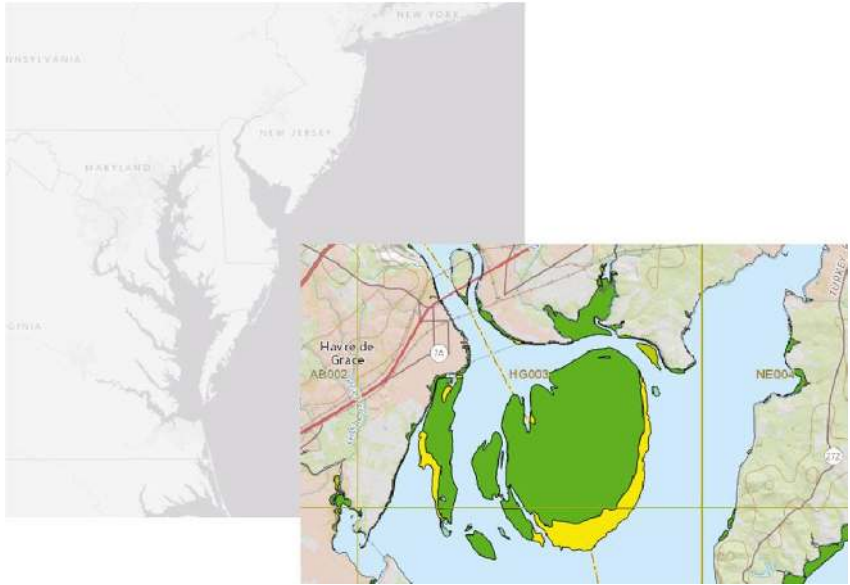
Figure 10. Areal image of the study site, Susquehanna Flats, taken in 2015 with an overlapping layer showing submerged aquatic vegetation density m on the bed (Virginia Institute of Marine Science: http://web.vims.edu/bio/sav/maps.html).

C	mass concentration of sediment fraction, kg/m^3;	p	fluid pressure, N/m^2;
C_b	vegetation drag coefficient, -;	Q	river discharge, m^3/s;
C_D	bottom roughness according with Chezy, m$^{\frac{1}{2}}$/s;	ρ	fluid density, kg/m^3;
C_{eq}	equilibrium sediment concentration, kg/m^3;	S	relative decay of the spatially averaged velocity, -;
C_{rs}	representative Chezy value for submersed vegetation, m$^{\frac{1}{2}}$/s;	s	basin slope, -;
D	stems diameter, m;	τ_b	bed shear stress, N/m^2;
D_{50}	sediment median grain size, μm;	τ_{bv}	bed shear stress in presence of vegetation, m/s;
ε_s	eddy diffusivities of sediment fraction, m^2/s;	τ_{max}	maximum bed shear stress, N/m^2;
f	Coriolis parameter, s^{-1};	τ_t	total shear stress, N/m^2;
f_s	reduction factor for submerged vegetation, -;	τ_v	shear stress due to the vegetation drag, N/m^2;
g	gravity acceleration, m/s^2;	T_s	adaptation time, s;
h	water depth, m;	τ_{xx}	fluid shear stress, N/m^2;
H_v	vegetation height, m;	U	time averaged x-direct fluid velocity, m/s;
i	slope, -;	U_c	x-component of the velocity on the bar top, m/s;
k	van Karman constant, -;	U_0	x-component of the velocity at the river mouth, m/s;
$L_{no\,veg}$	bar distance computed on non-vegetated bar, m;	U_{veg}	longitudinal velocity computed on vegetated bar, m/s;
L_{veg}	bar distance computed on vegetated bar, m;	V	time averaged y-direct fluid velocity, m/s;
m	vegetation density, m^{-1};	W	time averaged z-direct fluid velocity, m/s;
M	normalized suspended sediment mass, -;	w	river mouth width, m;
$M_{no\,veg}$	suspended sediment mass computed on non-vegetated bar, kg;	x	longitudinal direction, m;
M_{veg}	suspended sediment mass computed on vegetated bar, kg;	y	transversal direction, m;
n	number of stems for square meter, m^{-2};	z	elevation, m;

Table 1. Notatio

4.2 Models set up

The models simulate the hydrodynamic and sediment transport processes involved in the morphological evolution of a river mouth bar, in the presence of submersed aquatic vegetation on the bed. The numerical domain is a square (3 km x 3 km) in which there is a river flow through an inlet on the western side (Figure 11). The computational grid is composed of squared cells (30 m x 30 m), which are refined along the centerline, where each cell size is 30 m x 10 m. In the vertical direction, 7non- homogeneous sigma layers are used, decreasing the layer thickness (%) of the local water depth for each layer going down to the bottom. The bottom layer is characterized by a thickness equal to 3% of the depth at each point of the domain. In particular, at the river mouth the bottom layer measures 0.09 m.

A steady and constant discharge and equilibrium sediment concentration enter the domain from the river mouth. The sediment boundary conditions consist of sand-sized sediment with a single grain diameter that changes in different runs; sediment enters the domain in equilibrium concentration with the flow field (*Nardin et al., 2013*). Only sandy sediment is considered, because river mouths are generally composed of sand (*Fielding et al., 2005; Turner and Tester, 2006*), varying the grain size from 64μm to 350μm.

At the inlet, a constant input of 0.6 kg/m^3 of suspended sediments is imposed, like in Nardin et al. (2013). All sediment is characterized by a specific density of $2,650 \text{ kg/m}^3$ and dry bed density of $1,600 \text{ kg/m}^3$.

The northern, southern, and eastern boundaries are open and we assign a fixed water level (Figure 11).

A trapezoidal river channel with flow depth $h = 3 \text{ m}$ is incised into a non-erodible coastline. The bottom stress is modeled with Chézy's formulation using the constant Chézy value $C_D = 65\sqrt{m}/s$. The initial condition of the models consists of a constant bathymetry with 5 m of erodible sand on the basin bottom.

The suspended sediment eddy diffusivities are a function of the fluid eddy diffusivities and are calculated using horizontal large eddy simulation and grain settling velocity.

The horizontal eddy diffusivity coefficient is defined as the combination of the sub grid-scale horizontal eddy viscosity, computed from a horizontal large eddy simulation, and the

background horizontal viscosity, here set equal to $0.001 \text{ m}^2\text{s}^{-2}$ (*Nardin et al., 2016; Edmonds and Slingerland, 2010*).

To satisfy the numerical stability criteria of Courant-Frederichs-Levy, we use a time step $\Delta t = 0.15$ min (*Lesser et al., 2004*).

To decrease the simulation time a morphological scale factor of 50 is used in our models, considering that the final solution is not affected for values less than 200, as shown by sensitivity experiments. The morphological factor is a user device to multiply the deposition and erosion rate in each Δt.
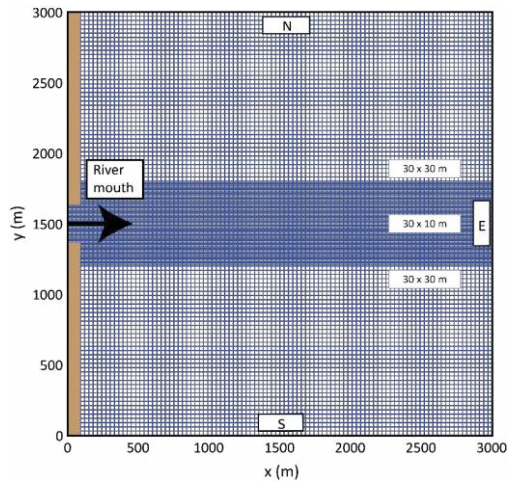
Figure 11. Computational domain and boundary conditions.

4.2.1 Bar formation set up

Previous studies show that bars typically start forming when the flow at the river mouth becomes unconfined (*Bates, 1953; Wang, 1984; Edmonds and Slingerland, 2007*); Edmonds and Slingerland (2007) demonstrate that the river mouth bar progrades basinward after its initial formation and then, when the bar stops prograding, it vertically aggrades and

58

stagnates. Stagnation occurs when the fluid pressure on the upstream side of the bar increases and the flow diverts around the bar due to significant reduction of velocity and shear stress over the bar top when the bar is 40% of the flow depth (*Edmonds and Slingerland, 2007*).

To study the effect of submersed aquatic vegetation on the morphological evolution of a river mouth bar, I first simulate bar formation without bed vegetation, like Edmonds and Slingerland (2007), using two different flow velocities at the inlet ($v_1 = 1\,\text{m/s}, v_2 = 1.5\,\text{m/s}$), varying the mouth width w, the basin slope s, and the sediment sand diameter (Table 2). Combining velocities and widths leads to four different discharges Q. For all simulations of bar formation, I imposed a spin-up time of 600 min to have fully developed hydrodynamics with a fixed bottom before any morphological changes happen in the numerical domain.

Run	**Q**	**w**	**s**	**D_{50}**	Run	**Q**	**w**	**s**	**D_{50}**
	($m^3 s^{-1}$)	(m)		(μm)		($m^3 s^{-1}$)	(m)		(μm)
T110125	600	200	0	125	T12064	1200	400	0	64
T111125	600	200	0.0001	125	T12164	1200	400	0.0001	64
T112125	600	200	0.001	125	T12264	1200	400	0.001	64
T11064	600	200	0	64	D120125	1800	400	0	125
T11164	600	200	0.0001	64	D121125	1800	400	0.0001	125
T11264	600	200	0.001	64	D122125	1800	400	0.001	125
D110125	900	200	0	125	D12064	1800	400	0	64
D111125	900	200	0.0001	125	D12164	1800	400	0.0001	64
D112125	900	200	0.001	125	D12264	1800	400	0.001	64
D11064	900	200	0	64	T110100	600	200	0	100
D11164	900	200	0.0001	64	T110125	600	200	0	125
D11264	900	200	0.001	64	T110200	600	200	0	200

T120125	1200	400	0	125	T110250	600	200	0	250
T121125	1200	400	0.0001	125	T110300	600	200	0	300
T122125	1200	400	0.001	125	T110350	600	200	0	350

Table 2. Boundaries and initial conditions used in Delft3D for the 30 numerical experiments of bar formation study

4.2.2 Vegetated bar models set up

For each run listed in Table 2, I obtained the bed level configurations corresponding to the instant at which every bar attained the value of 40% of the flow depth (h = 1.2 m), which represents the critical bar elevation when stagnation occurs (*Edmonds and Slingerland, 2007*). For convenience, I used the stagnant bar configuration to add submersed aquatic vegetation on the bar (Figure 12). In particular, I added submersed aquatic vegetation at all the points of the numerical domain where it can grow naturally, where the flow depth ranges from h = 0.5 − 1.6 m (*Abal and Dennison, 1996*).

I considered the stagnant configuration of each bar as the new initial condition for subsequent simulations of morphological evolution in the presence of submersed aquatic vegetation. Gurbisz et al. (2016) measured a suite of physical and biological processes in the large SAV bed of Susquehanna Flats, including plant biomass and flow velocities. Moreover, Gurbisz et al. (2016) stated that on Susquehanna Flat the best fit for submerged vegetation characteristics is obtained assuming the product of SAV density and height equals to 0.1. This calculation is being deduced supposing a slowly varying steady state shallow water balance between horizontal pressure gradient and vertical stress gradient, taking into account the influence of different friction, due to the presence of SAV.

In this study, I used several different vegetation densities (m = 1, 4, 7.5 m^{-1}) and deflected heights (H$_v$ = 0.1 − 0.8 m). The vegetation height and density values were chosen to be consistent with the field observations by Gurbisz et al. (2016), resulting in agreement with the velocity ratio between the flow observed at Susquehanna Flat in the SAV bed (~0.05 m/s) and in the non-vegetated channel (~0.13 m/s).

Also, this velocity values are used to account for the plant flexibility, in order to assign the SAV deflected height in our model. All the numerical results of the vegetated models were compared with non-vegetated models to quantify the impact of submersed aquatic vegetation on the morphological development of a river mouth bar. These different values of variables were combined to produce 340 different model run. Table 3 summarizes the main numerical experiments with submersed aquatic vegetation, considering the initial flat bathymetry.

Run	Q	w	D_{50}	H_v	m	Run	Q	w	D_{50}	H_v	m
	($m^3 s^{-1}$)	(m)	(µm)	(m)	(m^{-1})		($m^3 s^{-1}$)	(m)	(µm)	(m)	(m^{-1})
V11064	600	200	64	0.1	1	V11080	600	200	64	0.1	7.5
V11066	600	200	64	0.3	1	V11082	600	200	64	0.3	7.5
V11067	600	200	64	0.4	1	V11083	600	200	64	0.4	7.5
V11068	600	200	64	0.5	1	V11084	600	200	64	0.5	7.5
V11072	600	200	64	0.1	4	V110100	600	200	100	0.4	4
V11073	600	200	64	0.2	4	V110125	600	200	125	0.4	4
V11074	600	200	64	0.3	4	V110200	600	200	200	0.4	4
V11075	600	200	64	0.4	4	V110250	600	200	250	0.4	4
V11076	600	200	64	0.5	4	V110300	600	200	300	0.4	4
V11079	600	200	64	0.8	4	V110350	600	200	350	0.4	4

Table 3. Boundaries and initial conditions used in Delft3D for the main numerical models for the vegetated bar experiments
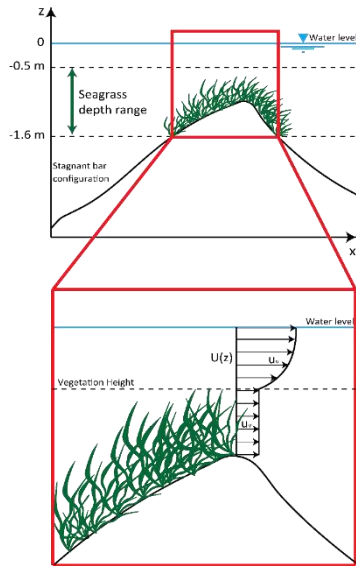
Figure 12. Schematization of the bed level corresponding to the stagnant bar configuration (Run ID T11064) with the seagrass depth range and velocity profile in the Delft 3D vegetation model for submersed vegetation (Baptist's formulation).

4.3 Results

4.3.1 Hydrodynamic results

To understand how vegetation impacts river mouth bar evolution, I first analyze the velocity field in the case of a stagnant bar configuration (Run ID: T11064). The bathymetry of this configuration is shown in Figure 13(a), where vectors show the magnitude of the depth-averaged velocity field predicted in the presence of submersed vegetation on the bar ($H_v = 0.4$ m, m=4 m^{-1}).

Considering the cross-section A, perpendicular to the centerline (Figure 13(a)), the velocity distribution in the presence of vegetation is compared with the test case without vegetation.

The longitudinal velocity, U-component, (Figure 13(b)) generally decreases on the bar in front of the river mouth, when the vegetation height and density increase. However, the longitudinal velocity increases laterally in the presence of vegetation.

The transverse velocity, V-component, (Figure 13(c)) is zero along the centerline and increases in the off-bar direction almost linearly moving toward the lateral side of the bar, when the vegetation height and density increase. The effect of vegetation produces an amplification of the peak off-bar velocity at cross-section A.

The longitudinal velocity U calculated along the centerline and normalized by the initial velocity Uo decreases approaching the top of the bar (Figure 14(a)). The normalized longitudinal velocity decreases much more for high values of vegetation height than for high values of vegetation density, shown by the more rapid decrease of velocity with increasing values of the height-density ratio. To quantify the relative decay of the depth-averaged velocity on the river mouth bar top induced by submersed aquatic vegetation, we define the jet spreading, S, as:

$$S = \frac{(U_o - U_c)_{veg}}{(U_o - U_c)_{no\,veg}} \qquad\qquad \text{Eq. 44}$$

where U_o and U_c are, respectively, the x-component velocities calculated on the river mouth and on the bar top. Comparing simulations of bar evolution in the presence of vegetation with

varying vegetation height and density, with the same bar evolution without vegetation, I find that the jet spreading S is a function of vegetation height H_v. In particular, jet spreading increases almost linearly with increased vegetation height and its density (Figure 14(b)), due to the decreased longitudinal velocity U_c on the river mouth bar due to the vegetation.

Figure 15 shows the bed shear stress τ for different vegetation conditions calculated along the centerline as a function of the longitudinal direction x (m) normalized with the value of the river mouth width w (m). Bed shear stress in the non-vegetated bar test case decreases toward the bar. In the vegetated scenarios, the bed shear stress decreases substantially because of the additional roughness imparted by the vegetation. Increasing vegetation height decreases τ more than increasing vegetation density.
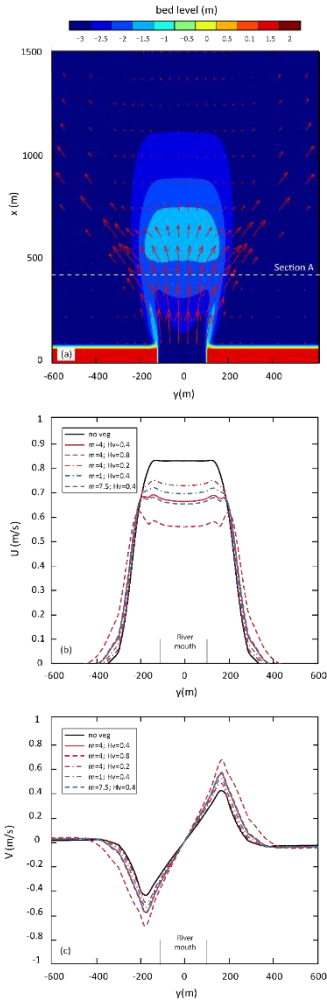
Figure 13. (a) Bathymetric contour map of the stagnant configuration and velocity magnitude vectors in the case of vegetated bar (H_v=0.4m; m=4m^{-1}); (b) longitudinal U and (c) transverse V depth averaged velocity along the transverse transect 400m, section A, from the river mouth, for different vegetation heights H_v and density m compared with the non-vegetated test case (solid black line). The lines parallel to the y axis delimit the river mouth width.
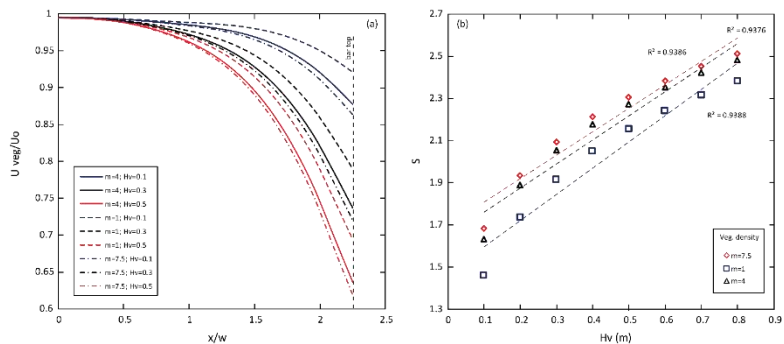
Figure 14. (a) Normalized longitudinal velocity along the centerline computed with different conditions of vegetation. (b) Relative decay of the average velocity S along the centerline as a function of the vegetation height for different values of density.
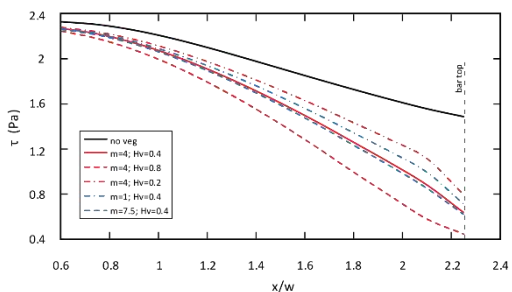
Figure 15. Bed shear stress calculated along the centerline for different vegetation conditions plotted as a function of the longitudinal direction x (m) normalized by the river mouth width w (m).

Vertical distributions of suspended-sediment concentration along the centerline are plotted in Figure 16(a) and (b) to illustrate the influences of vegetation on suspended-sediment transport. Without vegetation, the suspended-sediment concentration

distribution has high values near the bottom along the upstream side of the bar, enhancing vertical bar accretion (Figure 16(a)). In the presence of vegetation (Figure 16(b)), high values of suspended sediment concentration are confined upstream of the vegetated patch, where SSC is very low relative to the test case. Results show that the suspended-sediment concentration C decreases on the bar top when the vegetation height and density increases, compared with the non-vegetated test case. In both cases, the lowest values of SSC occur downstream of the bar.
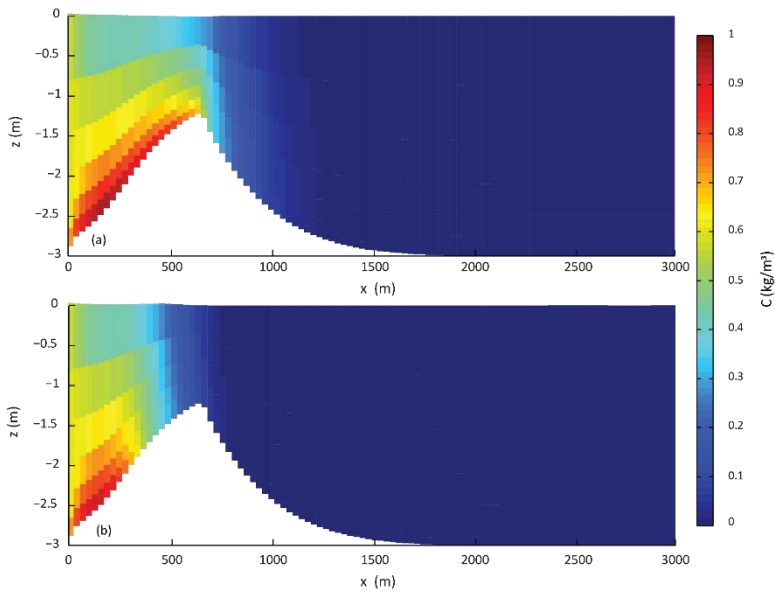
Figure 16. (a) Suspended-sediment concentration on the non-vegetated bar along the z-direction (depth) and (b) suspended-sediment concentration on the vegetated bar along the z-direction (submerged vegetation height H_v=0.4m, m= 4m^{-1}).

To further understand how the suspended-sediment concentration is influenced by the presence of submersed vegetation, I introduced the normalized suspended-sediment mass, M, defined as:

$$M = \frac{M_{veg}}{M_{noveg}} = \sum_i \frac{C_{veg,i} v_i}{C_{noveg,i} v_i}$$
<div align="right">Eq. 45</div>

where M_{veg} and M_{noveg} are the total amount of suspended sediment mass summed along the centerline model cells for the vegetated and non-vegetated bar, respectively, $C_{veg,\,i}$ are the mass concentrations of suspended sediment for the vegetated bar, $C_{noveg,\,i}$ are the mass concentrations of suspended sediment for the non-vegetated bar, v_i are the cell volumes, and subscript i represents all cells along the centerline.

Results show that normalized suspended-sediment mass decreases linearly when the vegetation height and density increases (Figure 17). This is probably because vegetation both decreases bottom shear stress and resuspension, and decreases sediment supply by diverting the flow laterally off-bar.

Figure 17. Normalized-suspended sediment mass along the centerline as a function of vegetation height for different density scenarios and linear regression lines plotted for each density.

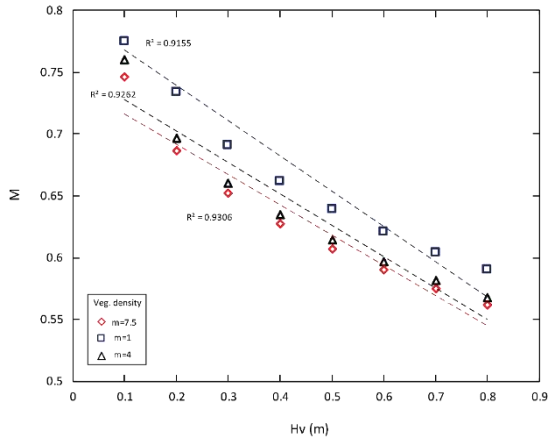*4.3.2 Morphodynamic results*

Submersed aquatic vegetation alters river mouth bar evolution mainly via additional hydraulic resistance to the flow, causing decreases in both velocity and maximum bed shear stress that change the distribution of suspended-sediment concentrations and thus, morphological bar evolution.

I analyzed morphology and position of bar development under the same conditions but in the presence or absence of vegetation. Our results show that the presence of submersed vegetation significantly changes the bar shape and position (Figure 18(a)). The green contour line represents the projection of initial bar configuration at section z = -1.6 m for the vegetated bar evolution; all points of the numerical domain inside the green patch are then vegetated only for the vegetated case.

The other lines show the bar location after 63 days of simulation for the non-vegetated (blue line) and vegetated (red line) cases corresponding to the z = -1 m contour.

The map shows that the vegetated bar evolves in the opposite direction of the non-vegetated bar and its shape appears smaller and less uniform than the other case. This suggests different development of the bar due to the effect of vegetation on sedimentary processes. Figure 18(b) and (c) show how the bar evolves every 2 days between days 55 and 63 of the simulation, starting from the same bed level (black line) corresponding with the stagnant configuration of the bar. The vegetated bar expands toward the river mouth forming a bump on its upstream side, near the vegetated patch limit, while the non-vegetated bar grows vertically and maintains its initial shape in the z-direction.

To quantify changes in the position of the bar, I normalized the distance of the vegetated bar L_{veg}, to the distance of the non-vegetated bar, L_{noveg}. The normalized distance from the river mouth decreases with increasing vegetation height for each value of vegetation density (Figure 19(a)), showing that vegetation height and density promote bar evolution toward the river mouth. The decrease in bar distance is due to the spreading effect on the velocity, shown in Figure 14. The spreading effect consists of a reduction of the velocity component along the main flow direction, caused by an increase in friction.
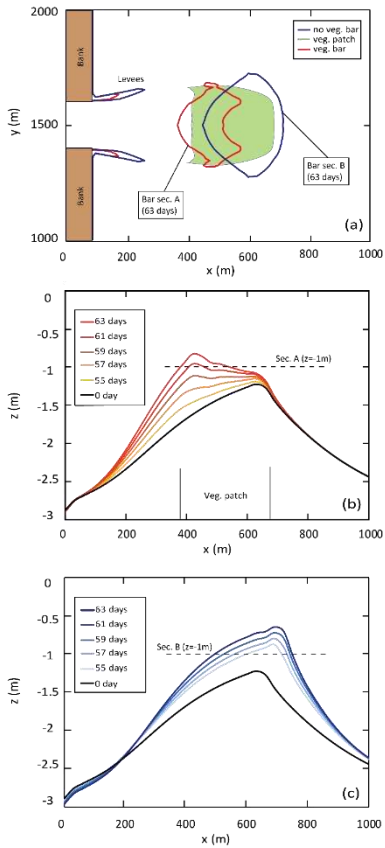
Figure 18. (a) Planview map of simulated locations of the non-vegetated bar (blue line) and the vegetated bar (red line; Hv=0.4m, m=4m-1) after 63 days of simulation for the contour z=-1m. The green shaded region indicates the initial location of the bar with the vegetated patch (Hv=0.4m, m=4m-1) at the section z=-1m. (b) Bed level evolution of the vegetated bar and (c) non-vegetated bar every two days calculated along the centerline.
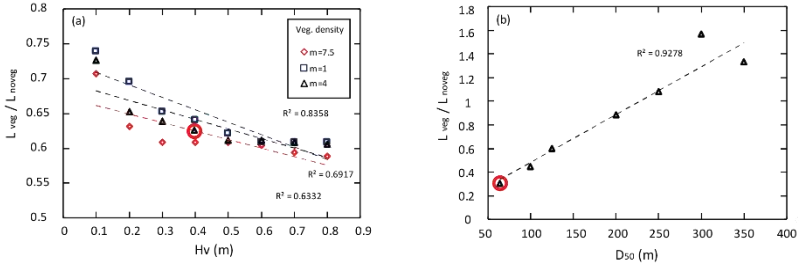
Figure 19. Normalized bar distance from the river mouth along the centerline as a function of (a) vegetation height and >(b) sediment grain size in the presence of submersed vegetation characterized by Hv=0.4m and m=4m-1. The red circle markers in the figures represent the same study case.

Therefore, the flow diverts with an increase of the transversal component of the velocity. This is because deposition of sediments is governed by gradients in velocity, so that if the longitudinal velocity decreases because of the friction due to the vegetation presence on the bottom, then part of the sediment in suspension settles at the bed. As a result, more spreading triggers deposition closer to the mouth. In addition, Figure 19(b) indicates that the normalized bar distance increases linearly with sediment grain size, for a vegetation height of 0.4 m and density 4 m^{-1} on the bar.

To evaluate the threshold vegetation characteristic at which the presence of vegetation becomes dynamically significant to move the bar downstream, I plotted the sediment flux crossing the bar peak (Figure 20) as a function of the total submerged vegetation volume per square meter V_t, defined as:

$$V_t = V_{ss}\, n \qquad\qquad \text{Eq. 46}$$

$$V_{ss} = \pi \left(\frac{D}{2}\right)^2 H_v \qquad\qquad \text{Eq. 47}$$

where V_{ss} is the vegetation stems volume.

In order to show the variability across scales, I plotted the variable V_t in logarithmic scale.

Figure 20 indicates that the sediment flux is inversely proportional to the increment of V_t. For very low values of V_v, the sediment flux over the bar decreases but the bar continues to migrate upstream, until the tipping point corresponding to the $V_t=5\times10^{-5}$ (red mark in Figure 20), when the trend reverses. Past the tipping point, the sediment flux decreases much more until it becomes constant and downstream bar migration occurs.

The black dashed line in Figure 20 represents the switching trend of the bar, crossing the tipping point.
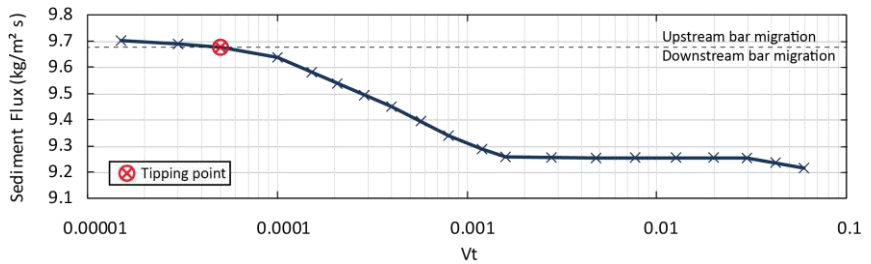

Figure 20. Sediment flux crossing the bar peak as a function of the total submerged vegetation volume per square meter Vv. The red mark represents the tipping point and the black dashed line indicates the switching trend of the bar crossing the tipping point.

5.   Discussion and conclusions

5.1   Discussion

5.1.1 Comparison with previous models

The presence of vegetation cover significantly affects the spatial sedimentation patterns that drive the morphological evolution of the idealized river mouth bar. Plants introduce additional hydraulic resistance to the flow, decreasing the velocity through and near the vegetated patch relative to the non-vegetated scenario. Suspended-sediment transport decreases because of the reduction in bed shear stress, modifying the sediment distribution.

This study highlights the important role of the river discharge, the amount of suspended-sediment concentration, and submersed vegetation height and density on river mouth bar morphology.

Previous work by Nardin et al. (2013) and Leonardi et al. (2013) showed how waves and tidal currents might be able to increase river jet expansion. They relate the jet spreading to an increased shear stress on top of the bar. My results show similar behavior of the jet spreading due to an increased roughness on the bar due to SAV.

Moreover, Wright (1977) highlighted the important role of bottom friction on the rapid expansion of the jet and the subsequent deposition of sediments. My results quantify these two mechanisms in a process-based framework: SAV increases turbulent bed friction that slows down the river-mouth jet, triggering expansion and mouth-bar formation close to the outlet.

In real cases, SAV would be able to encroach the new sediment deposits. However, my initial sensitivity analysis investigated the possible propagation of the SAV in the new zone according to the simulated timescale. In fact, simulations explored a short-term evolution and even if the SAV could start to colonize, my runs are not long enough in time.

In addition, extreme events causing massive erosion or deposition of sediments can cause the death of entire SAV populations. The sediment underlying an SAV bed in Florida was completely eroded away and redeposited elsewhere (*Hine et al., 1987*). On the other

73

extreme, high sedimentation rates can also be responsible for the decline of SAV populations. This study neglects the hypothetical SAV colonization.

5.1.2 Seasonality effects on river mouth bar morphodynamics

To discuss insights from the idealized vegetated bar to its dynamic morphological evolution, I investigated the bar development for different seasons. This study focuses on evaluating the location of sediment deposition and erosion for varying discharge and submersed vegetation characteristics.

All values were chosen using the unvegetated study case (ID T11064, Table II) as the reference condition and by increasing or decreasing values by 50% from the reference conditions to represent reasonable seasonal changes. I chose seasonal changes of 50% considering that the Susquehanna River discharge measured at Conowingo Station (USGS 01578310) varies seasonally between 23% and 113%. And, for example, the measured discharge at Wax Lake Delta from 2009 to 2012 varies around 30–100%, as shown in Nardin and Edmonds (2014). Thus, changing values by 50% seems reasonable for understanding the sedimentation patterns of our idealized model.

Annual variations of vegetation height and density taken into account by the model are chosen to be consistent with the seasonal biomass measured by Gurbisz et al. (2016) on the Susquehanna Flats.

The unvegetated case is used to simulate winter, when submersed vegetation is absent due to cold temperatures. In this case, the bar grows vertically, prograding in the offshore direction, and sediment deposition occurs on the bar top (Figure 21(a)).

To simulate spring, I used a higher discharge (Q= 920 m³/s) with submersed vegetation height of 0.4 m. During the spring simulation (Figure 21(b)), water flow is hindered and sediment is trapped by the vegetation, causing deposition on the vegetated patch and on its upstream side. This pattern of sedimentation results in bar progradation in the opposite direction to that in winter, moving toward the river mouth starting from the same bar configuration. The increment of sedimentation rate during the spring is due to the high river discharge.

During summer, river discharge usually decreases (Q =230 m³/s) but the vegetation height increases (Hv =0.8 m). The lower discharge results in deposition upstream of the vegetated

patch, because the submersed vegetation represents an obstacle to both water and sediment flux (Figure 21(c)).

A seasonal sequence of bar evolution can be run, using the winter configuration as the initial condition for the spring simulation, the resulting spring configuration as the initial configuration for the summer simulation, and the summer configuration for the fall simulation. Results show that the spring conditions are most responsible for the final configuration, causing sediment deposition on the bar top through the vegetated patch (Figure 21(d)). However, the three separated seasons shown in Figure 21(a), (b), (c) behave slightly differently from the seasonal succession in Figure 21(d) due to the different initial set up of the seasons.
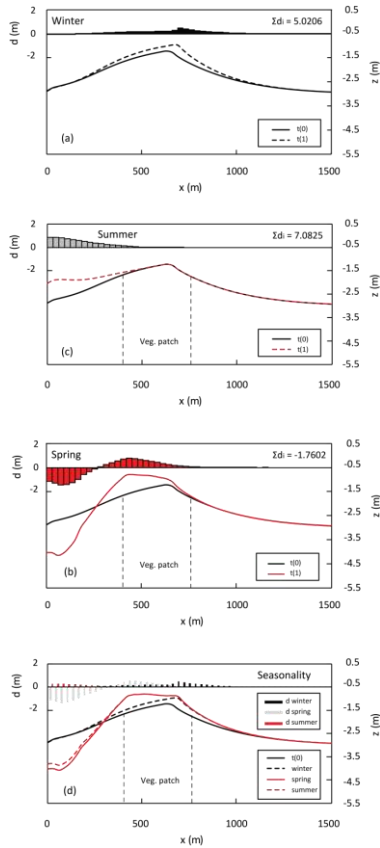
Figure 21. Bed level evolution with the corresponding accretion rate of sediment deposition and erosion during (a) the winter, (b) the spring and (c) the summer, varying the initial conditions of suspended sediment concentration, discharge and the presence or absence of submerged vegetation on the bar; (d) progressive bed level evolution during the alternating seasons with the corresponding accretion rate of sediment deposition and erosion for every season.

76

5.1.3 Applicability of the results to the Susquehanna Flats

An example of the morphological influence of submersed aquatic vegetation is observed at the Susquehanna River mouth. Upper Chesapeake Bay hydrology is dominated by Susquehanna River outflow (*Schubel and Pritchard, 1986*) and, based on the results of this study, the presence of SAV at the river mouth significantly influences the sediment distribution at the Bay inlet.

However, the amount of sediment supplied by the Susquehanna has been dramatically reduced since construction of the Conowingo Dam (~16 km from the upper Bay) in 1928, especially impacting the supply of sand.

For this reason, I can compare the numerical results from the vegetated bar only with historical bathymetry of the Flats from 1799 to Conowingo Dam construction, rather than its recent morphology. A report from 1899 by the Officer of US Coastal and Geodetic Survey, responsible for the hydrographic survey, describes the extensive SAV bed at Susquehanna Flats.

In addition, navigation charts by NOAA (National Oceanic and Atmospheric Administration) provide historical bathymetry. A sequence of navigation charts of the study area is presented in Figure 22 to show morphological changes of the bar in different years.

The images show that the distance of the Flats from the river mouth decreases over time, indicating upstream migration of the bar similar to our numerical results.

Moreover, Gurbisz et al. (2017) measured the flow velocity during high SAV biomass (June) and low SAV biomass (August). The mean current speed was 57% less (0.07 vs 0.03 m/s) within the SAV bed in August compared with May–June. Current speed was 69% less within the vegetated bed compared with the non-vegetated channel in May–June and 88% less in August. Gurbisz et al. (2017) showed that the presence of submerged vegetation on the Susquehanna Flat reduces the velocity by three times. This is in agreement with our results shown in Figure 14.
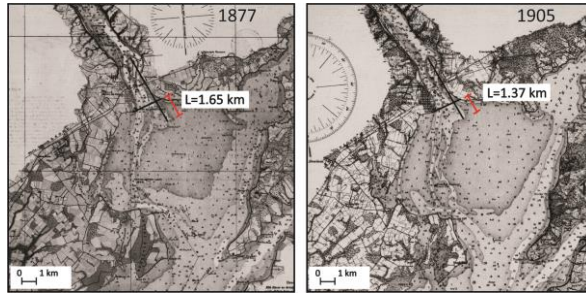
Figure 22. Historical bathymetry of Susquehanna Flats (Navigation charts by NOAA: http://historicalcharts.noaa.gov/historicals) and the measured bar distance from the Susquehanna River mouth.

5.1.4 Comparing model results to the other study systems

Islands in the Wax Lake Delta are shaped like arrowheads pointing upstream, with two contiguous levees extending downstream in smoothly (*Shaw et al., 2013*). Islands are colonized by plant communities and vegetation is distributed across an island depending on the fraction of the year that a particular location is inundated by water (*Johnson et al., 1985; Viparelli et al., 2011*). The islands of the Wax Lake Delta are very prominently shaped like the vegetated bar plan-view obtained from our idealized model in Figure 18(a).

Therefore, those results suggest that the vegetation strongly influences the morphological evolution of river dominated delta. A sedimentological examination of the Wax Lake (*Majersky et al., 1997; Majersky-Fitzgerald, 1998*) and Atchafalaya deltas (*van Heerden and Roberts, 1980*) indicates that they are very similar with regard to sedimentary architecture and they are both vegetated. Roberts (1998) showed the eastern lobe of the Atchafalaya delta in two different years and the images illustrate growth of the delta by vertical accretion and upstream growth, as this model suggests.

5.2 Conclusion

Understanding river mouth bar development is crucial for predicting delta evolution.

To investigate on the effect of vegetation on the development of river mouth bars, in this study Delft3D is chosen because this is the most stabilized numerical model to represent and analyze large scale and long term processes with a good compromise with computational grid and simulation time.

In this study I investigated the effect of SAV on the morphological development of a river mouth bar. The presence of vegetation on the bar top decreased the longitudinal velocity over the top of the developing bar and increased the transverse velocity over the bar, resulting in a velocity redistribution around the bar. Increasing the vegetation height and density decreased the bed shear stress over the bar, resulting in a reduction of sediment transport.

Therefore, the submersed vegetation led to a different morphological bar configuration. In the absence of vegetation, the bar aggraded vertically and its peak prograded toward the basin. In the presence of SAV, less sediment reached the bar top because of the increased roughness of SAV, enhancing sedimentation before the vegetated patch.

This sediment distribution implied a bar progradation toward the river mouth, in the opposite direction to the unvegetated bar. Increasing SAV height and density reduced the distance from the river mouth to the bar deposit.

Future research might explore interactive feedbacks between morphodynamics and emergent vegetation, development of channels through the bar, or grass bed patchiness.

References

Abal, EG, WC Dennison (1996), Seagrass depth range and water quality in southern Moreton Bay, Queensland, Australian Mar. Fresh. Res. 47: 763-771.

Abdelrhman, M. A. (2007). Modeling coupling between eelgrass Zostera marina and water flow. Marine Ecology Progress Series, 338, 81-96.

Arboleda, A. M., Crosato, A. and Middelkoop, H. (2010), Reconstructing the early 19th-century Waal River by means of a 2D physics-based numerical model. Hydrol. Process., 24: 3661-3675. doi:10.1002/hyp.7804

Afzalimehr, H., & Subhasish, D. E. Y. (2009). Influence of bank vegetation and gravel bed on velocity and Reynolds stress distributions. International Journal of Sediment Research, 24(2), 236-246.

Axelsson, V. (1967), The Laitaure Delta: A Study of Deltaic Morphology and Processes. Geografiska Annaler. Series A, Physical Geography, 49(1), 1-127. doi:10.2307/520865.

Baptist, M. J., Van den Bosch, L. V., Dijkstra, J. T. and Kapinga, S. (2005), Modelling the Effects of Vegetation on Flow and Morphology in Rivers, Archiv. Hydrobiol. Suppl., 155: 1–4. Large Rivers 15(1–4), 339–357.

M.J. Baptist, V. Babovic, J. Rodríguez Uthurburu, M. Keijzer, R.E. Uittenbogaard, A. Mynett & A. Verwey (2007) On inducing equations for vegetation resistance, Journal of Hydraulic Research, 45:4, 435-450, DOI: 10.1080/00221686.2007.9521778

Barnes, H. H. (1967). Roughness characteristics of natural channels (No. 1849). US Government Printing Office.

Bates, C. C., (I953) Rational theory of delta formation, Bull. Am. Ass. Petr. Geol., vol. 37 no. 9, Tulsa.

Belcher SE, Harman IN, Finnigan JJ. 2012. The wind in the willows: flows in forest canopies in complex terrain. Annu. Rev. Fluid Mech. 44: 479–504

Bennett, E. L. (2002). Is there a link between wild meat and food security?. Conservation Biology, 16(3), 590-592.

Bennett, S. J., Wu, W., Alonso, C. V., & Wang, S. S. (2008). Modeling fluvial response to in-stream woody vegetation: implications for stream corridor restoration. Earth Surface Processes and Landforms: The Journal of the British Geomorphological Research Group, 33(6), 890-909.

Bijvelds, M. D. J. P. (2001), Numerical modelling of estuarine flow over steep topography, PhD thesis, Delft Univ. of Technol, Delft, Netherlands

Brown G, Roshko A. 1974. On density effects and large structure in turbulent mixing layers. J. Fluid Mech. 64: 775–816

Burke, R. W., & Stolzenbach, K. D. (1983). Free surface flow through salt marsh grass.

Canestrelli, A., S. Fagherazzi, A. Defina, and S. Lanzoni (2010), Tidal hydrodynamics and erosional power in the Fly River delta, Papua New Guinea, J. Geophys. Res., 115, F04033, doi:10.1029/2009JF001355.

Carollo, F. G., Ferro, V. I. T. O., & Termini, D. (2002). Flow velocity measurements in vegetated channels. Journal of Hydraulic Engineering, 128(7), 664-673.

Chambers PA, Kalff J. 1985. Depth distribution and biomass of submersed aquatic macrophyte communities in relation to Secchi depth. Can. J. Fish. Aquat. Sci. 42: 701–9

Charnley PR. 1987. Lowland drainage. In River Engineering. Part I, Design Principles, Brandon TW (ed.). The Institution of Water Engineers and Scientists: London; 173–224.

Chow, V. T. (1959). Open-channel hydraulics. NY etc.

Costanza, R., Fisher, B., Ali, S., Beer, C., Bond, L., Boumans, R., ... & Gayer, D. E. (2008). An integrative approach to quality of life measurement, research, and policy. SAPI EN. S. Surveys and Perspectives Integrating Environment and Society, (1.1).

Crosato, A. and Saleh, M. S. (2011), Numerical study on the effects of floodplain vegetation on river planform style. Earth Surf. Process. Landforms, 36: 711-720. doi:10.1002/esp.2088

Dackombe, R. V., & Gardiner, V. (1983). Geomorphological field manual. Allen & Unwin.

D'Alpaos, A., S. Lanzoni, M. Marani, and A. Rinaldo (2007), Landscape evolution in tidal embayments: Modeling the interplay of erosion, sedimentation, and vegetation dynamics, J. Geophys. Res., 112, F01008, doi:10.1029/2006JF000537.

Darby, S. E. (1999). Effect of riparian vegetation on flow resistance and flood potential. Journal of hydraulic engineering, 125(5), 443-454.

Defina, A., & Bixio, A. C. (2005). Mean flow and turbulence in vegetated open channel flow. Water Resources Research, 41(7).

De Swart, H.E., Zimmerman, J.T.F., (2009), Morphodynamics of tidal inlet systems, Annual Review of Fluid Mechanics 41, 203–229.

Dijkstra J.T. (2008), How to account for flexible aquatic vegetation in large-scale morphodynamic models in: Smith JM (ed.) International Conference on Coastal Engineering 2008, Hamburg, p 2820-2831.

Dijkstra, J. T., & Uittenbogaard, R. E. (2010). Modeling the interaction between flow and highly flexible aquatic vegetation. Water Resources Research, 46(12).

Edmonds, D. A. (2012), Stability of backwater influenced bifurcations: A study of the Mississippi-Atchafalaya bifurcation, Geophys. Res. Lett., 39, L08402, doi:10.1029/2012GL051125.

Edmonds, D. A., and R. L. Slingerland (2007), Mechanics of river mouth bar formation: Implications for the morphodynamics of delta distributary networks, J. Geophys. Res., 112, F02034, doi:10.1029/2006JF000574.

Edmonds DA, Slingerland RL. (2010). Significant effect of sediment cohesion on delta morphology. Nat. Geosci. 3:105–9.

Edmonds, D. A., Hoyal, D., Sheets, B. A. & Slingerland, R. L., (2009), Predicting delta avulsions: Implications for coastal wetland restoration. Geology 37, 57 759–762.

Edmonds, D.A., Shaw, J.B., and Mohrig, D., (2011), Topset-dominated deltas: a new model for river delta stratigraphy: Geology, v. 39, p. 1175–1178.

Esposito, C. R., I. Y. Georgiou, and A. S. Kolker (2013), Hydrodynamic and geomorphic controls on mouth bar evolution, Geophys. Res. Lett., 40, 1540–1545, doi:10.1002/grl.50333.

Eckman JE (1990) A model of passive settlement by planktonic larvae onto bottoms of differing roughness. Limnol Oceanogr 35,887-901

Fagherazzi S, Overeem I. (2007), Models for deltaic and inner continental shelf landform evolution, Annu. Rev. Earth Planet. Sci., 35:685–715.

Fernandez-Illescas, C. P., & Rodriguez-Iturbe, I. (2004). The impact of interannual rainfall variability on the spatial and temporal patterns of vegetation in a water-limited ecosystem. Advances in Water Resources, 27(1), 83-95.

Fielding, C. R., J. D. Trueman, and J. Alexander (2005), Sharp-based, flood-dominated mouth bar sands from the Burdekin River delta of northeastern Australia: Extending the spectrum of mouth-bar facies, geometry, and stacking patterns, J. Sediment. Res., 75, 55 – 66.

Finnigan, J. (2000). Turbulence in plant canopies. Annual review of fluid mechanics, 32(1), 519-571.

Fischer-Antze, T., Stoesser, T., Bates, P., & Olsen, N. R. B. (2001). 3D numerical modelling of open-channel flow with submerged vegetation. Journal of Hydraulic Research, 39(3), 303-310.

Fitzmaurice L, Shaw RH, Paw U KT, Patton EG. 2004. Three-dimensional scalar microfront systems in a large-eddy simulation of vegetation canopy flow. Bound.-Layer Meteorol. 112: 107–27

FitzGerald D.M., Buynevich I.V., Argow B., (2006), A coupled model of tidal inlet and barrier island dynamics in a regime of accelerated sea-level rise, J. Coast. Res., SI 39:789–795.

Folkard, A. M. (2011). Vegetated flows in their environmental context: a review. Proceedings of the Institution of Civil Engineers-Engineering and Computational Mechanics, 164(1), 3-24.

Gac, J. M. (2014). A large eddy based lattice-Boltzmann simulation of velocity distribution in an open channel flow with rigid and flexible vegetation. Acta Geophysica, 62(1), 180-198.

Gambi, M. C., Nowell, A. R., & Jumars, P. A. (1990). Flume observations on flow dynamics in Zostera marina(eelgrass) beds. Marine ecology progress series. Oldendorf, 61(1), 159-169.

Geleynse, N., J. E. A. Storms, M. J. F. Stive, H. R. A. Jagers, and D. J. R. Walstra (2010), Modeling of a mixed-load fluvio-deltaic system, Geophys. Res. Lett., 37, L05402, doi:10.1029/2009GL042000.

Geleynse, N., J. E. A. Storms, D. J. R. Walstra, H. R. A. Jagers, Z. B. Wang, and M. J. F. Stive (2011), Controls on river delta formation; insights from numerical modelling, Earth Planet. Sci. Lett., 302, 217– 226. doi:10.1016/j.epsl.2010.12.013.

Ghisalberti M. 2000. Mixing layers and coherent structures in vegetated aquatic flows. MS thesis. Mass. Inst. Technol. 126 pp.

Ghisalberti M, Nepf H. 2002. Mixing layers and coherent structures in vegetated aquatic flow. J. Geophys. Res. 107(C2): 3011

Ghisalberti M, Nepf H. 2004. The limited growth of vegetated shear layers. Water Resour. Res. 40: W07502

Ghisalberti M, Nepf H. 2005. Mass transfer in vegetated shear flows. Environ. Fluid Mech. 5: 527–51

Ghisalberti M, Nepf H. 2009. Shallow flows over a permeable medium: the hydrodynamics of submerged aquatic canopies. Transp. Porous Media 78: 385–402

Green, J. C. (2005). Modelling flow resistance in vegetated streams: review and development of new theory. Hydrological Processes: An International Journal, 19(6), 1245-1259.

Gosselink, J., & Pendleton, E. C. (1984). The ecology of delta marshes of coastal Louisiana: a community profile. Louisiana State Univ Baton Rouge Center For Wetland Resources.

Gurbisz, C., and W.M. Kemp. (2014), Unexpected resurgence of a large submersed plant bed in Chesapeake Bay: Analysis of time series data, Limnology and Oceanography 59:482-498, doi:10.4319/1o.2014.59.2.0482.

Gurbisz, C., W. M. Kemp, L. P. Sanford, and R. J. Orth. (2016), Mechanisms of storm-related loss and resilience in a large submersed plant bed, Estuaries and Coasts: 951-966, doi:10.1007/s12237-016-0074-4.

Gurbisz, C., Kemp, W.M., Cornwell, J.C. et al. Estuaries and Coasts (2017) 40: 1626. https://doi.org/10.1007/s12237-017-0249-7.

Gurnell, A. M., Petts, G. E., Hannah, D. M., Smith, B. P., Edwards, P. J., Kollmann, J., ... & Tockner, K. (2001). Riparian vegetation and island formation along the gravel-bed Fiume Tagliamento, Italy. Earth Surface Processes and Landforms: The Journal of the British Geomorphological Research Group, 26(1), 31-62.

Gurnell, A., Tockner, K., Edwards, P., & Petts, G. (2005). Effects of deposited wood on biocomplexity of river corridors. Frontiers in Ecology and the Environment, 3(7), 377-382.

Hey, R. D., Flow resistance in gravel-bed rivers, J. Hydraul. Eng., 105, 365 – 379, 1979.

Hine, A.C., M. Evans, R. Davis, Jr., and D. Belknap. 1987. Depositional response to seagrass mortality along a low-energy, barrier island coast: west central Florida. Journal of Sedimentary Petrology 57: 431-439.

Hydraulics, D. (2001). Delft3D user interface, Capabilities and applications. Delft Hydraulics, Delft.

Howard, J. A., & Mitchell, C. W. (1985). Phytogeomorphology. John Wiley & Sons.

Huang, Y. H., Saiers, J. E., Harvey, J. W., Noe, G. B., & Mylon, S. (2008). Advection, dispersion, and filtration of fine particles within emergent vegetation of the Florida Everglades. Water Resources Research, 44(4).

Ikeda, S., Yamada, T. and Toda, Y. (2001). "Numerical Study on Turbulent Flow and Honami in and above Flexible Plant Canopy". Int. J. Heat Fluid Flow 22, 252–258.

Järvelä, J. (2004). Determination of flow resistance caused by non-submerged woody vegetation. International Journal of River Basin Management, 2(1), 61-70.

Järvelä, J. (2005). Effect of submerged flexible vegetation on flow structure and resistance. Journal of Hydrology, 307(1-4), 233-241.

Jenter, H. L., & Duff, M. P. (1999). Locally-forced wind effects on shallow waters with emergent vegetation. In Proc. Third Int. Symp. Ecohydraulics. IAHR.

Jerolmack, D. J. (2009), Conceptual framework for assessing the response of delta channel networks to Holocene sea level rise, Quat. Sci. Rev., 28(17-18), 1786–1800.

Jerolmack, D. J., and J. B. Swenson (2007), Scaling relationships and evolution of distributary networks on wave-influenced deltas, Geophys. Res. Lett., 34, L23402, doi:10.1029/2007GL031823.

Jimenez J. 2004. Turbulent flows over rough walls. Annu. Rev. Fluid Mech. 36: 173–96

Johnson W.B., Sasser C.E., Gosselink J.G., (1985), Succession of vegetation in an evolving river delta, Atchafalaya Bay, Louisiana, J. Ecol., 73:973–86.

Kaimal J, Finnigan J. 1994. Atmospheric Boundary Layer Flows: Their Structure and Measurement. New York: Oxford Univ. Press. 289 pp.

Kim, W. (2012), GEOMORPHOLOGY: Flood-built land, Nat. Geosci., 5(8), 521–522.

Kim, W., Mohrig, D., Twilley, R., Paola, C., & Parker, G. (2009). Is it feasible to build new land in the Mississippi River Delta?. Eos, Transactions American Geophysical Union, 90(42), 373-374.

Kirkby, M. J., Atkinson, K., & Lockwood, J. O. H. N. (1990). Aspect, vegetation cover and erosion on semi-arid hillslopes (pp. 25-39). John Wiley and Sons Ltd..

Kubrak, e., kubrak, j., & rowiński, p. M. (2008). Vertical velocity distributions through and above submerged, flexible vegetation. Hydrological sciences journal, 53(4), 905-920.

Inoue E. 1963. On the turbulent structure of airflow within crop canopies. J. Meteorol. Soc. Jpn. 49: 121–24

Laio, F., A. Porporato, L. Ridolfi, and I. Rodriguez-Iturbe (2001), Plants in water-controlled ecosystems: Active role in hydrologic processes and response to water stress: II. Probabilistic soil moisture dynamics, Adv. Water Resour., 24(7), 707 – 723.

Lanzoni, S., and G. Seminara (2002), Long-term evolution and morphodynamic equilibrium of tidal channels, J. Geophys. Res., 107(C1), 1–13, doi:10.1029/2000JC000468.

Laurel G. Larsen and Judson W. Harvey, (2010), How Vegetation and Sediment Transport Feedbacks Drive Landscape Change in the Everglades and Wetlands Worldwide., The American Naturalist 176, no. 3: E66-E79.

Lawson et al. 2012. Enhancement of sediment suspension and nutrient flux by benthic macrophytes at low biomass. Mar. Ecol. Prog. Ser. Vol. 448: 259–270.

Leendertse, J. J. (1990). Discussion of "Turbulence Modeling of Surface Water Flow and Transport: Part III" by the ASCE Task Committee on Turbulence Models in Hydraulic Computations (September, 1998, Vol. 114, No. 9). Journal of Hydraulic Engineering, 116(4), 600-602.

Leonard, L., and M. Luther, Flow hydrodynamics in tidal marsh canopies, Limnol. Oceanogr., 40, 1474-1484, 1995.

Leonard, L. A., & Croft, A. L. (2006). The effect of standing biomass on flow velocity and turbulence in Spartina alterniflora canopies. Estuarine, Coastal and Shelf Science, 69(3-4), 325-336.

Leonardi, N., A. Canestrelli, T. Sun, and S. Fagherazzi (2013), Effect of tides on mouth bar morphology and hydrodynamics, J. Geophys. Res. Oceans, 118, doi:10.1002/jgrc.20302.

Lesser, G. R., J. A. Roelvink, J. A. T. M. van Kester, and G. S. Stelling (2004), Development and validation of a three-dimensional morphological model, Coastal Eng., 51(8–9), 883–915.

Li, C. W., & Xie, J. F. (2011). Numerical modeling of free surface flow over submerged and highly flexible vegetation. Advances in Water Resources, 34(4), 468-477.

Lightbody, A. F., & Nepf, H. M. (2006). Prediction of velocity profiles and longitudinal dispersion in salt marsh vegetation. Limnology and oceanography, 51(1), 218-228.

Liu, C., and H. Nepf (2016), Sediment deposition within and around a finite patch of model vegetation over a range of channel velocity, Water Resour. Res., 52, 600–612, doi:10.1002/ 2015WR018249.

Lòpez, F., and Garcia, M. (1998), Open-channel flow through simulated vegetation: Suspended sediment transport modeling., Water Res. Res., 34(9), 2341–2352.

Luhar et al. 2008. Interaction between flow, transport and vegetation spatial structure. Env. Fluid Mech. 8(5-6):423-39.

Macdonald R, Griffiths R, Hall D. 1998. An improved method for the estimation of surface roughness of obstacle arrays. Atmos. Environ. 32: 1857–64

Majersky, S., H.H. Roberts, R. Cunningham, G.P. Kemp, and C.J. John, 1997, Facies development in the Wax Lake Outlet delta: Present and future trends: Basin Research Institute Bulletin 7, p. 50-66.

Majersky-Fitzgerald, S., 1998. The development and sand body geometry of the Wax Lake Outlet Delta, Atchafalaya Bay, Loui- siana. Ms Thesis, Department of Oceanography and Coastal Sci- ences, Louisiana State University, Baton Rouge, Louisiana, 130p

Moore, 2004. Influence of seagrasses on water quality in shallow regions of the lower Chesapeake Bay, J. of Coastal Res., 20:162-178.

Mossa, M., Ben Meftah, M., De Serio, F., & Nepf, H. M. (2017), How vegetation in flows modifies the turbulent mixing and spreading of jets, Scientific Reports, 7, 6587. http://doi.org/10.1038/s41598-017-05881-1.

Murphy E, Ghisalberti M, Nepf H. 2007. Model and laboratory study of dispersion in flows with submerged vegetation. Water Resour. Res. 43: W05438

Naylor, L. A., Viles, H. A., & Carter, N. E. A. (2002). Biogeomorphology revisited: looking towards the future. Geomorphology, 47(1), 3-14.

Naiman RJ, Johnston CA, Kelley JC (1988) Alteration of North American streams by beaver. BioScience 38:753–762

Naiman, R. J., & Decamps, H. (1997). The ecology of interfaces: riparian zones. Annual review of Ecology and Systematics, 28(1), 621-658.

Nardin, W. & Edmonds, D.A. (2014) Optimum vegetation height and density for inorganic sedimentation in deltaic marshes, Nature Geoscience, 7, 722–726.

Nardin, W., and S. Fagherazzi (2012), The effect of wind waves on the development of river mouth bars, Geophys. Res. Lett., 39, L12607, doi:10.1029/2012GL051788.

Nardin, W., G. Mariotti, D. A. Edmonds, R. Guercio, and S. Fagherazzi (2013), Growth of river mouth bars in sheltered bays in the presence of frontal waves, J. Geophys. Res. Earth Surf., 118, 872–886, doi:10.1002/jgrf.20057.

W. Nardin, D.A. Edmonds, S. Fagherazzi, 2016, Influence of vegetation on spatial patterns of sediment deposition in deltaic islands during flood, Advances in Water Resources, Volume 93, Part B, Pages 236-248, ISSN 0309-1708 https://doi.org/10.1016/j.advwatres.2016.01.001.

Nepf, H. M., (1999), Drag, turbulence and diffusion in flow through emergent vegetation, Water Resources Research 35:479– 489.

Nepf H, Ghisalberti M, White B, Murphy E. 2007. Retention time and dispersion associated with submerged aquatic canopies. Water Resour. Res. 43: W04422

Nepf, H., & Ghisalberti, M. (2008). Flow and transport in channels with submerged vegetation. Acta Geophysica, 56(3), 753-777.

Nepf, H. M., Sullivan, J. A., & Zavistoski, R. A. (1997). A model for diffusion within emergent vegetation. Limnology and Oceanography, 42(8), 1735-1745.

Nepf, H. M., & Vivoni, E. R. (2000). Flow structure in depth-limited, vegetated flow. Journal of Geophysical Research: Oceans, 105(C12), 28547-28557.

Nepf, H. M., & Koch, E. W. K. (1999). Vertical secondary flows in submersed plant-like arrays. Limnology and oceanography, 44(4), 1072-1080.

Nicholls, R. J., & Mimura, N. (1998). Regional issues raised by sea-level rise and their policy implications. Climate research, 11(1), 5-18.

Nittrouer, J. A., Shaw, J., Lamb, M. P., & Mohrig, D. (2012). Spatial and temporal trends for water-flow velocity and bed-material sediment transport in the lower Mississippi River. Bulletin, 124(3-4), 400-414.

Nikora, N. F., & Nikora, V. I. (2007). A viscous drag concept for flow resistance in vegetated channels.

Nikora, V. (2010). Hydrodynamics of aquatic ecosystems: an interface between ecology, biomechanics and environmental fluid mechanics. River research and applications, 26(4), 367-384.

Osterkamp, W. R., & Hupp, C. R. (1996). 17 The Evolution of Geomorphology, Ecology, and Other Composite Sciences. In The Scientific Nature of Geomorphology: Proceedings of the 27th Binghamton Symposium in Geomorphology, Held 27-29 September, 1996 (Vol. 27, p. 415). John Wiley & Sons.

Overeem I, Syvitski JPM, Hutton EWH. ,(2005), Three-dimensional numerical modeling of deltas. In River Deltas: Concepts, Models and Examples, ed. JP Bhattacharya, L Giosan, SEPM Spec. Publ. 83:13–30. Tulsa.

Okamoto T, Nezu I. 2009. Turbulence structure and monami phenomena in flexible vegetated open-channel flows. J. Hydraul. Res. 47: 798–810

Paola, C., R. R. Twilley, D. A. Edmonds, W. Kim, D. Mohrig, G. Parker, E. Viparelli, and V. R. Voller (2011), Natural processes in delta restoration: Application to the Mississippi Delta, Annu. Rev. Mar. Sci., 3, 67–91, doi:10.1146/annurev-marine-120709-142856.

Partheniades, E., (1965), Erosion and deposition of cohesive soils, J. Hydraul. Div. Am. Soc. Civ. Eng., 91, 105- 139.

Piomelli, U., Balaras, E., 2002. Wall-layer models for large-eddy simulations. Annu. Rev. Fluid Mech. 34 (1), 349–374.

Phillips, J. D. (1999). Edge effects in geomorphology. Physical Geography, 20(1), 53-66.

Pitlo, R. H. (1986). Towards a larger flow capacity of vegetated channels. In Proceedings EWRS/AAB 7th Symposium on Aquatic weeds.

Poggi, D., Katul, G. G., & Albertson, J. D. (2004). A note on the contribution of dispersive fluxes to momentum transfer within canopies. Boundary-layer meteorology, 111(3), 615-621.

Pope, S.B., 2000. Turbulent Flows. Cambridge University Press.

Porporato, A., Laio, F., Ridolfi, L., & Rodriguez-Iturbe, I. (2001). Plants in water-controlled ecosystems: active role in hydrologic processes and response to water stress: III. Vegetation water stress. Advances in Water Resources, 24(7), 725-744.

Porporato, A., D'odorico, P., Laio, F., & Rodriguez-Iturbe, I. (2003). Hydrologic controls on soil carbon and nitrogen cycles. I. Modeling scheme. Advances in Water Resources, 26(1), 45-58.

Powell Jr, J. A. (1978). Evidence of carnivory in manatees (Trichechus manatus). Journal of Mammalogy, 59(2), 442-442.

Raupach, M. R., & Shaw, R. H. (1982). Averaging procedures for flow within vegetation canopies. Boundary-Layer Meteorology, 22(1), 79-90.

Raupach, M., Finnigan, J. J., & Brunet, Y. (1996). Coherent eddies and turbulence in vegetation canopies: the mixing-layer analogy. In Boundary-layer meteorology 25th anniversary volume, 1970–1995 (pp. 351-382). Springer, Dordrecht.

Roelvink, J. A., and G. K. Van Banning (1994), Design and development of DELFT3D and application to coastal morphodynamics, in Hydroinformatics, edited by Babovic and Maksimovic, pp. 451–456, Rotterdam, Balkema.

Roberts, H. (1998). Delta Switching: Early Responses to the Atchafalaya River Diversion. Journal of Coastal Research, 14(3), 882-899. Retrieved from http://www.jstor.org/stable/4298842

Rominger, J. T., Lightbody, A. F., & Nepf, H. M. (2010). Effects of added vegetation on sand bar stability and stream hydrodynamics. Journal of Hydraulic Engineering, 136(12), 994-1002.

Rosen, T. & Xu, Y. J., (2013), Recent decadal growth of the Atchafalaya River Delta complex: Effects of variable riverine sediment input and vegetation succession. Geomorphology 194, 108–120.

Russ, E.R. and C.M. Palinkas (2018), Seasonal-scale and decadal-scale sediment-vegetation interactions on the subaqueous Susquehanna River delta, upper Chesapeake Bay. Estuaries and Coasts. DOI: 10.1007/s12237-018-0413-8.

Siniscalchi, F., & Nikora, V. I. (2012). Flow-plant interactions in open-channel flows: A comparative analysis of five freshwater plant species. Water Resources Research, 48(5).

Schulz, M., Rinke, K., & Köhler, J. (2003). A combined approach of photogrammetrical methods and field studies to determine nutrient retention by submersed macrophytes in running waters. Aquatic Botany, 76(1), 17-29.

Schubel, J.R. & Pritchard, D.W. Estuaries (1986) Responses of upper Chesapeake Bay to variations in discharge of the Susquehanna River, 9: 236. https://doi.org/10.2307/1352096

Shaw, J. B., D. Mohrig, and S. K. Whitman (2013), The morphology and evolution of channels on the Wax Lake Delta, Louisiana, USA, J. Geophys. Res. Earth Surf., 118, 1562–1584, doi:10.1002/jgrf.20123.

Shimizu Y, Tsujimoto T. 1994. Numerical analysis of turbulent open-channel flow over a vegetation layer using a k-ε turbulence model. J. Hydrosci. Hydraul. Eng. 11: 57–67

Souliotis D, Prinos P (2011) Effect of a vegetation patch on turbulent channel flow. J Hydraul Res 49(2):157–167

Stallins, J. A. (2006). Geomorphology and ecology: unifying themes for complex systems in biogeomorphology. Geomorphology, 77(3-4), 207-216.

Stelling, G. S., & Van Kester, J. A. T. M. (1994). On the approximation of horizontal gradients in sigma co-ordinates for bathymetry with steep bottom slopes. International Journal for Numerical Methods in Fluids, 18(10), 915-935.

Steiger, J., Tabacchi, E., Dufour, S., Corenblit, D., & Peiry, J. L. (2005). Hydrogeomorphic processes affecting riparian habitat within alluvial channel–floodplain river systems: a review for the temperate zone. River Research and Applications, 21(7), 719-737.

Stoesser, T., Liang, C., Rodi, W., Jirka, G.H. (2006). Large eddy simulation of fully-developed turbulent flow through submerged vegetation. Proceedings of River Flow 2006 1, 227–234.

Stoesser, T., Kim, S. J., & Diplas, P. (2010). Turbulent flow through idealized emergent vegetation. Journal of Hydraulic Engineering, 136(12), 1003-1017.

Syvitski, J. P., Vörösmarty, C. J., Kettner, A. J., & Green, P. (2005). Impact of humans on the flux of terrestrial sediment to the global coastal ocean. science, 308(5720), 376-380.

Sukhodolova, T. A., & Sukhodolov, A. N. (2012). Vegetated mixing layer around a finite-size patch of submerged plants: 1. Theory and field experiments. Water Resources Research, 48(10).

Sun, T., C. Paola, G. Parker, and P. Meakin, (2002), Fluvial fan deltas: Linking channel processes with large-scale morphodynamics, Water Resour. Res., 38(8), doi:10.1029/2001WR000284.

Tabacchi, E., Lambs, L., Guilloy, H., Planty-Tabacchi, A. M., Muller, E., & Decamps, H. (2000). Impacts of riparian vegetation on hydrological processes. Hydrological processes, 14(16-17), 2959-2976.

Tanino, Y., & Nepf, H. M. (2008). Laboratory investigation of mean drag in a random array of rigid, emergent cylinders. Journal of Hydraulic Engineering, 134(1), 34-41.

Tanino, Y., & Nepf, H. M. (2008). Lateral dispersion in random cylinder arrays at high Reynolds number. Journal of Fluid Mechanics, 600, 339-371.

Temmerman, S. et al. (2007), Vegetation causes channel erosion in a tidal landscape. Geology 35, 631–634.

Tennekes, H., Lumley, J. L., & Lumley, J. L. (1972). A first course in turbulence. MIT press.

Thorne, C.R. (1990). Effects of Vegetation on Riverbank Erosion and Stability in Vegetation and Erosion, edited by Thornes, J.B., John Wiley, New York, 125–144.

Turner, B.R., And Tester, G.N., (2006), The Table Rocks Sandstone: a fluvial, friction dominated lobate mouth bar sandbody in the Westphalian B Coal Measures, NE England: Sedimentary Geology, v. 190, p. 97–119.

Uittenbogaard, R. (2003). "Modelling Turbulence in Vegetated Aquatic Flows". International Workshop on riparian forest Vegetated Channels: Hydraulic, Morphological and Ecological Aspects, Trento, Italy, 20–22 February 2003.

Van Heerden, I.L. And Roberts, H.H., 1988. Facies development of Atchafalaya Delta, Louisiana: A modern bayhead delta. Amer- ican Association Petroleum Geologists Bulletin, 72, 439-453.

van Katwijk et al. 2010. Sediment modification by seagrass beds: muddification and sandification induced by plant cover and environmental conditions. Est., Coastal, Shelf Sci. doi:10.1016/j.ecss.2010.06.008.

Van Wijk, M. T., & Rodriguez-Iturbe, I. (2002). Tree-grass competition in space and time: Insights from a simple cellular automata model based on ecohydrological dynamics. Water Resources Research, 38(9), 18-1.

Van Rijn, L. C., (1993), Principles of sediment transport in rivers, estuaries, and coastal seas, Aqua Publications, Blokzijl, The Netherlands.

Viles, H. A. (Ed.). (1988). Biogeomorphology. B. Blackwell.

Villada Arroyave, J. A., & Crosato, A. (2010). Effects of river floodplain lowering and vegetation cover. Proceedings of the ICE-Water Management, 163 (9), 2010.

Viparelli, E., D. Gaeuman, P. Wilcock, and G. Parker (2011), A model to predict the evolution of a gravel bed river under an imposed cyclic hydrograph and its application to the Trinity River,
Water Resour. Res., 47, W02533, doi:10.1029/2010WR009164.

Wang, F. C. (1984), The dynamics of a river-bay-delta system, J. Geophys. Res., 89(C5), 8054–8060, doi:10.1029/JC089i C05p08054.

White B, Nepf H. 2003. Scalar transport in random cylinder arrays at moderate Reynolds number. J. Fluid Mech. 487: 43–79

Winant C, Browand F. 1974. Vortex pairing: the mechanism of turbulent mixing-layer growth at moderate Reynolds number. J. Fluid Mech. 63: 237–55

Wright, L. D. (1977), Sediment transport and deposition at river mouths: A synthesis, Geol. Soc. Am. Bull., 88(6), 857–868, doi:10.1130/0016- 7606(1977)882.

Wright, L. D., and J. M. Coleman (1974), Mississippi river mouth processes: Effluent dynamics and morphologic development, J. Geol., 82(6), 751–778. doi:10.2307/30078268.

Zong, L., Nepf, H. (2010), Flow and deposition in and around a finite patch of vegetation, Geomorphology 116 (3–4), 363–372.

Ringraziamenti

A conclusione di questo elaborato, vorrei dedicare uno spazio a chi, con dedizione e pazienza, ha contribuito alla sua realizzazione.

Un sentito grazie al mio relatore, *Prof. Ing. Roberto Guercio*, per i suoi indispensabili consigli e per le conoscenze trasmesse durante questi tre anni di ciclo di dottorato. Grazie perché ha saputo guidarmi, sia come maestro di vita sia con consigli pratici, nella vita come nella ricerca.

Un ringraziamento speciale invece al *Prof. William Nardin*, il mio Advisor durante il periodo di ricerca trascorso presso Horn Point Laboratory – University of Maryland Center for Environmental Science. Lo ringrazio per avermi seguita in maniera assidua e costante per un anno e mezzo, per avermi trasmesso gran parte delle sue conoscenze, per avermi stimolato e appassionato al lavoro e per aver avuto la pretesa che presto avrei camminato sulle mie gambe. Colgo l'occasione per ringraziarlo anche per avermi sostenuto quotidianamente al di fuori del lavoro, facendomi sentire quasi a casa anche oltreoceano.

Fondamentali sono state anche tutte le persone con cui ho condiviso il mio tempo a Cambridge, in Maryland, in particolar modo Juan, Miles, Corinne, Iacopo e Alessandro. Già lì sapevo di aver incontrato amici speciali, che avrei sempre portato nel cuore, e cercavo di ricambiare il loro affetto offrendo molto spesso degustazioni di cucina italiana (gli americani apprezzano!). Ricorderò sempre le birre, i tornei di ping-pong, le serate di luna piena e *"That '70s Show"*.

Un importante ringraziamento è rivolto anche agli amici-colleghi del XXXII ciclo di Dottorato in Ingegneria Idraulica e Ambientale, un gruppo che è stato particolarmente ed inaspettatamente legato sin dai primi giorni. Grazie quindi a Vincenzo, Camilla, Andrea M., Francesco, Andrea N., per le risate e l'affetto condivisi sia in dipartimento che fuori. Mai avrei pensato che persone tanto diverse potessero essere tanto aperte e complici come lo siamo noi.

Ringrazio di cuore le mie amiche più strette, Miranda e Silvia, che hanno sempre creduto in me e che mi hanno spinto a non mollare nei momenti più duri, che hanno preteso che io ce la facessi, che hanno ascoltato e sopportato in silenzio tutti i miei lamenti, che sono state presenti anche mentre ero all'estero, cercando di non farmi mai sentire lontana. A loro che ci sono da sempre, nei momenti di bisogno, di paranoia e di follie, di risate e di pianti, di gastrite e di yoga, di camomilla e di vino rosso, un grazie così grande che solo voi sapete e che piango scrivendolo.

E ci tengo a ringraziare anche il gruppo dei nuovi colleghi, che condividono con me la gioia di questo traguardo che sto per raggiungere, ed il mio nuovo gruppo di amici *"Non di Milano"* con cui il giovedì (come oggi) ho appuntamento da Rino per un aperitivo, ma non stasera che sono qui a ringraziarvi!!

E ancora grazie, a tutte le persone che ho incontrato nel mio percorso di ricerca e non, negli ultimi tre anni, tutti i nuovi amici e le nuove conoscenze, perché ognuno a modo proprio ha contribuito a rendere il mio percorso di crescita lavorativo e personale più ricco, sia per le esperienze condivise, sia per gli insegnamenti ricevuti.

Un grazie speciale a mio fratello Gabri, perché ogni volta che mi guarda con quegli occhi mi fa capire che è fiero di me, e confesso che questo è gran parte della mia forza.

Ho lasciato per ultimo il ringraziamento più importante e più difficile. Ringrazio mamma e papà per avermi insegnato la costanza e il sacrificio, dandomi sempre affetto anche se a modo loro, e talvolta non lo capivo. E grazie soprattutto per avermi fatta così testarda, perché altrimenti non avrei mai raggiunto questo traguardo.

Grazie